NRL Report 7673

# Oceanic Horizontal Random Temperature Structure

W. B. Moseley and D. R. Del Balzo

*Large Aperture Systems Branch*
*Acoustics Division*

July 25, 1974

**NAVAL RESEARCH LABORATORY**
**Washington, D.C.**

Approved for public release; distribution unlimited.

SECURITY CLASSIFICATION OF THIS PAGE (When Data Entered)

| REPORT DOCUMENTATION PAGE | | READ INSTRUCTIONS BEFORE COMPLETING FORM |
|---|---|---|
| 1. REPORT NUMBER<br>NRL Report 7673 | 2. GOVT ACCESSION NO. | 3. RECIPIENT'S CATALOG NUMBER |
| 4. TITLE (and Subtitle)<br>OCEANIC HORIZONTAL RANDOM TEMPERATURE STRUCTURE | | 5. TYPE OF REPORT & PERIOD COVERED<br>Interim report<br>6. PERFORMING ORG. REPORT NUMBER |
| 7. AUTHOR(s)<br>W.B. Moseley and D.R. Del Balzo | | 8. CONTRACT OR GRANT NUMBER(s) |
| 9. PERFORMING ORGANIZATION NAME AND ADDRESS<br>Naval Research Laboratory<br>Washington, D.C. 20375 | | 10. PROGRAM ELEMENT, PROJECT, TASK AREA & WORK UNIT NUMBERS<br>NRL Problem S01-55<br>RR 031-03-41-5910 |
| 11. CONTROLLING OFFICE NAME AND ADDRESS<br>Department of the Navy<br>Office of Naval Research<br>Arlington, Virginia 22217 | | 12. REPORT DATE<br>July 25, 1974<br>13. NUMBER OF PAGES<br>56 |
| 14. MONITORING AGENCY NAME & ADDRESS(if different from Controlling Office) | | 15. SECURITY CLASS. (of this report)<br>UNCLASSIFIED<br>15a. DECLASSIFICATION/DOWNGRADING SCHEDULE |

16. DISTRIBUTION STATEMENT (of this Report)

Approved for public release; distribution unlimited.

17. DISTRIBUTION STATEMENT (of the abstract entered in Block 20, if different from Report)

Interim report

18. SUPPLEMENTARY NOTES

19. KEY WORDS (Continue on reverse side if necessary and identify by block number)

Thermal microstructure
Buoyancy
Spatial spectra
Brunt-Väisälä frequency
Anisotropic turbulence

20. ABSTRACT (Continue on reverse side if necessary and identify by block number)

A theoretical model of the horizontal spatial distribution of thermal microstructure is developed for anisotropic turbulence. A two-term power law representation for buoyancy and convective forces is applicable for wavenumbers greater than those of the internal wave field, but less than those in the dissipation range. The model predicts a temperature power density spectrum which decays as −5/3 and −3 in the convective and buoyancy ranges, respectively. The relative power in the two ranges is a function of depth and depends on the total rate of energy dissipation, the total rate of dissipation of temperature variance, and the Brunt-Väisälä frequency. Companion

(Continued)

DD FORM 1 JAN 73 1473 EDITION OF 1 NOV 65 IS OBSOLETE
S/N 0102-014-6601



SECURITY CLASSIFICATION OF THIS PAGE (When Data Entered)

experimental data from 54 long horizontal tows at depths between 97.5 and 1454 m at two widely separated stations in the Bermuda area of the North Atlantic verify the theoretical predictions.

## CONTENTS

INTRODUCTION . . . . . 1

HISTORICAL BACKGROUND . . . . . 2

Velocity Spectrum . . . . . 2
Temperature Spectrum . . . . . 4

THEORETICAL DEVELOPMENT . . . . . 7

DATA ANALYSIS . . . . . 12

COEFFICIENT STUDY . . . . . 18

AN OVERVIEW OF OCEANIC TEMPERATURE FLUCTUATIONS . . . . . 23

CONCLUSIONS . . . . . 24

REFERENCES . . . . . 24

APPENDIX A—Instrumentation, Experimental Techniques, and Data Reduction . . . . . 26

APPENDIX B—Temperature Power Spectral Density Plots . . . . . 34

APPENDIX C—Instability of Medium . . . . . 49

LIST OF SYMBOLS . . . . . 53

# OCEANIC HORIZONTAL RANDOM TEMPERATURE STRUCTURE

## INTRODUCTION

Over the last decade, a considerable amount of effort by a number of researchers has been devoted to the measurement of the random horizontal temperature structure of the oceans. This effort has produced a variety of power law* characterizations of this structure. The following references provide an indication of the scope of the disparity in the empirical power law representations.

Hecht and White (1) studied temperature fluctuations in the frequency range 3-30 cycles/hr with their ship drifting midway between Madeira and the Azores and with temperature sensors at depths of 5, 15, 25, 35, 45, and 112 m. Least-squares analysis gave power laws ranging from -2.6 to -3.4.

Neshyba, Neal, and Denner (2) obtained temperature profiles (at successive 4-min intervals) between 200 and 250 m in the Arctic Ocean with a thermistor. Results from their 30-hr time series at depths of 212 and 247 m reveal a power law of -3 for frequencies greater than the Brunt-Väisälä frequency.

Temperature data gathered by a self-propelled underwater research vehicle in the North Pacific at various depths between 40 and 2500 m were analyzed and reported by McKean (3). In the wavenumber range $0.03\ \mathrm{m}^{-1} < k < 3.14\ \mathrm{m}^{-1}$ his temperature spectra "behave approximately like $k^{-2}$."

While towing a chain of thermistors, E. C. LaFond (4) obtained data on the displacement of isotherms in the North Pacific. He reports power laws ranging between -1.75 and -2.65 for the 15°C and 18°C isotherms in the frequency range of 0.6 to 24 cycles/hr.

Black (5) towed this same thermistor chain over the continental shelf off California and performed structure function analyses at 34 depths evenly spaced from the surface to 750 ft. His results, when converted to power spectrum notation, show power laws between -1.66 and -2.23.

Temperature data obtained by Moseley and Del Balzo (6) from a towed platinum resistance thermometer at depths between 500 and 1100 m in the North Atlantic provide power laws between -1.97 and -2.26 for $0.02\ \mathrm{m}^{-1} < k < 0.64\ \mathrm{m}^{-1}$.

---

Note: Manuscript submitted October 16, 1973.

*When power spectral density $T$ as a function of wavenumber $k$ has the form $T = ak^b$, the exponent $b$ is commonly referred to as the power law.

The large-scale thermal structure was studied by Voorhis and Perkins (7) with a towed thermistor at 100 m depth near Bermuda. They saw a $\rho^{2/3}$ dependence in their structure function formulation which corresponds to a -5/3 power law for $0.0002\ m^{-1} < k < 0.06\ m^{-1}$.

The works cited above were deliberately chosen because they are concerned with spectral ranges not usually associated with the more established low-wavenumber, linear, internal wave range or the high-wavenumber, isotropic turbulence range. This intermediate range is treated in great detail both theoretically and experimentally in this report. It is shown that buoyancy forces have a depth-dependent effect on a certain size of scales of the temperature microstructure spectrum which can result in a wide range of power law representations. The form of the temperature power spectral density curve, which is developed and verified throughout the intermediate wavenumber range, is strongly influenced by the Brunt-Väisälä frequency.

## HISTORICAL BACKGROUND

Theoretical analyses of random temperature structure have often been made under the assumption that temperature is a passive additive quantity; i.e., it is carried by but does not contribute to the water motion. It is therefore appropriate to discuss briefly the velocity spectrum of the underlying dynamic mechanism, the fluid movement.

### Velocity Spectrum*

The three-dimensional velocity spectrum of a turbulent nonstratified fluid can be described (see Fig. 1a) in order of increasing wavenumber by (a) a low wavenumber range wherein the turbulent energy is established, (b) a range dominated by large stable eddies, (c) an inertial range (assuming a sufficiently large Reynolds number) where the turbulent motion is homogeneous and isotropic and where energy cascades toward higher wavenumbers, and (d) a viscous energy dissipation range where shear forces damp the motion. The form of the velocity spectrum in the inertial range (as derived by Kolmogorov (8) is

$$V_I(k) = \alpha\, \epsilon_0^{2/3}\, k^{-5/3}, \tag{1}$$

where $\alpha$ is an absolute constant, $\epsilon_0$ is the total rate of energy dissipation, $k$ is the wavenumber, and the subscript $I$ refers to the inertial range. Batchelor (9) and Hinze (10) give thorough accounts of homogeneous isotropic turbulence.

Now, consider a stably stratified medium, such as the ocean, where turbulence is assumed isotropic in horizontal planes only. The velocity spectrum in the inertial range may be modified by the mean density gradient. In fact, an internal wave range and a buoyancy range exist in the velocity spectrum between large stable eddies and inertial turbulence (see Fig. 1b). The velocity spectrum of the turbulence throughout the combined buoyancy-inertial range is given by

*The velocity spectrum is often denoted *energy* spectrum since it refers to kinetic energy fluctuations.

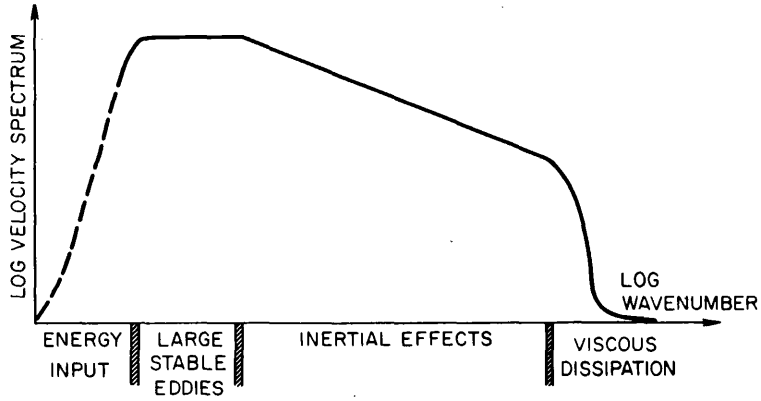


(a)

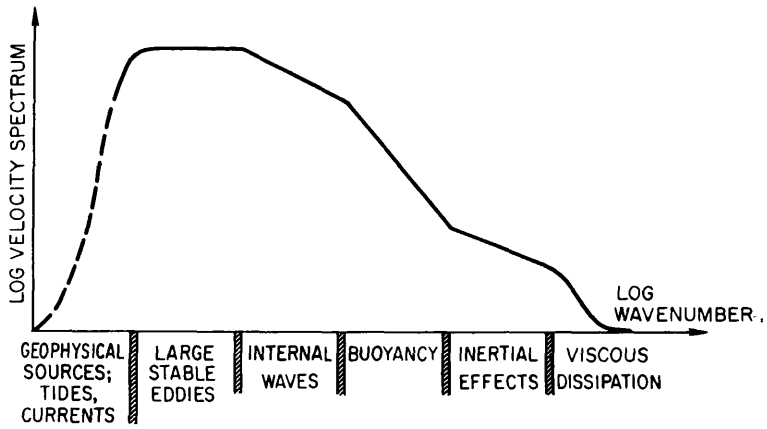


(b)

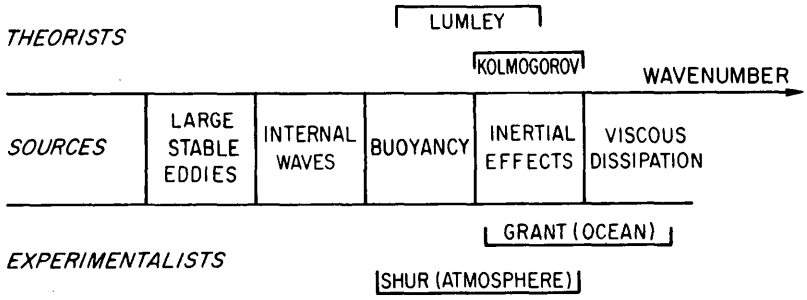


(c)

Fig. 1—Velocity spectrum (a) of an unlayered turbulent fluid, (b) of a turbulent stratified ocean, (c) theoretical and experimental contributors.

$$V_{BI}(k) = \alpha[\epsilon(k)]^{2/3}\, k^{-5/3}, \tag{2}$$

where

$$[\epsilon(k)]^{2/3} = \epsilon_0^{2/3}\left[1 + \left(\frac{k_b}{k}\right)^{4/3}\right], \tag{3}$$

$$k_b = C^{3/4} N^{3/2} \epsilon_0^{-1/2}, \tag{4}$$

$C$ is a positive constant, $N$ is the Brunt-Väisälä frequency, $k_b$ is representative of the transition range between buoyancy and inertial effects, $\epsilon$ is the net rate of spectral energy transfer from wavenumbers less than $k$ to wavenumbers greater than $k$, and the subscript $BI$ refers to the buoyancy-inertial range. These equations were first derived by Lumley (11). A more complete discussion of the velocity spectrum of ocean turbulence is given by Phillips (12).

Several facts about the buoyancy-inertial range should be noted. It is the basic anisotropy of the stably stratified medium which produces the buoyancy and thus the statistical properties of the motion in the range are anisotropic. Two basic underlying assumptions are (a) the rate at which energy is transferred through wavenumber $k_0$ (and not through distant wavenumbers) is a determining factor of the stratistical properties of the motion at the same wavenumber; and (b) in a stably stratified ocean, the buoyancy spectrum is assumed proportional to the local mean density gradient or $N^2$.

The buoyancy-inertial formulas are applicable when $k$ is large compared to wavenumbers associated with large stable eddies and small compared to dissipation wavenumbers. Energy considerations require that buoyancy-range motion is turbulent and cannot be regarded as an ensemble of interacting free internal waves.

Shur (13) has experimentally observed the spectral division between buoyancy and inertial effects for high-altitude aircraft measurements of turbulence in a stably stratified atmosphere. Observations have been made in the high-wavenumber inertial and dissipation ranges with a hot film flowmeter in a tidal channel by Grant, Stewart, and Moilliet (14) and in the open ocean by Grant, Hughes, Vogel, and Moilliet (15). Current meter measurements in the inertial range were taken by Webster (16). Figure 1c summarizes the various ranges of the velocity spectrum, along with the theoretical and experimental contributors.

## Temperature Spectrum

One might suspect a direct relationship between the thermal environment and the turbulent velocities. The theoretical development of the fluctuating temperature structure in a turbulent medium has, in fact, followed directly the analysis of the fluctuating velocity field. The power spectrum of random temperature fluctuations in a nonlayered, turbulent environment can be described (see Fig. 2a) in order of increasing wavenumber by (a) a low-wavenumber range wherein temperature variance is established, (b) a convective range (assuming a sufficiently high Péclet number) where temperature variance

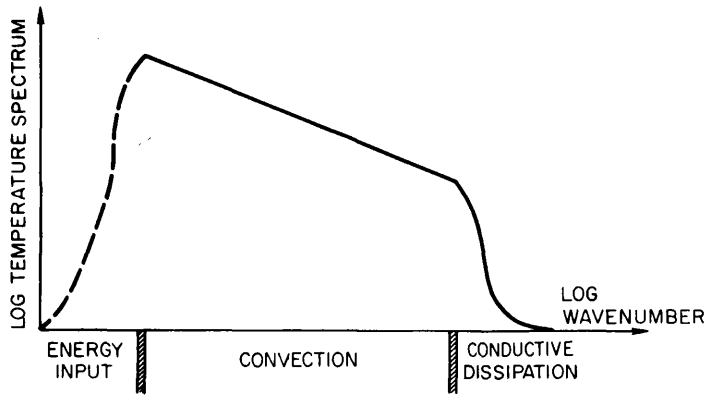


(a)

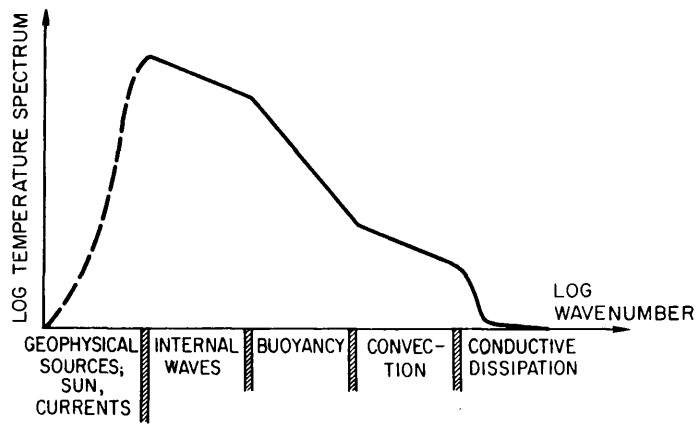


(b)

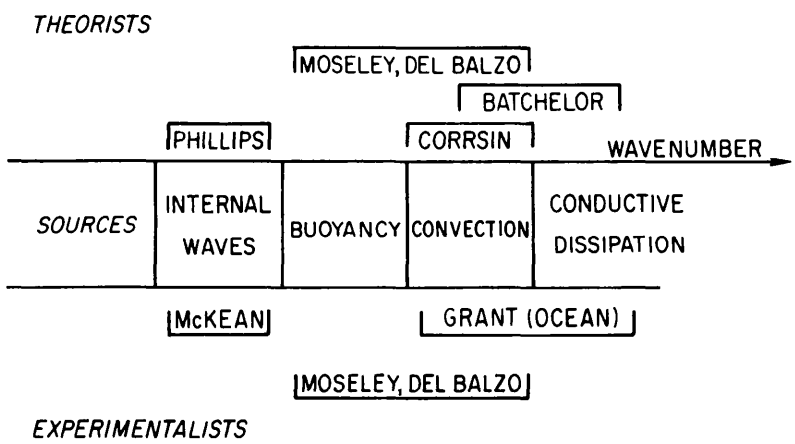


(c)

Fig. 2—Temperature spectrum (a) of an unlayered turbulent fluid, (b) of a turbulent stratified ocean (c) theoretical and experimental contributors.

cascades toward higher wavenumbers, and (c) a dissipation range where the temperature variance is eliminated by conduction.

The form of the temperature power density spectrum in the convective range was derived by Obukhov (17) and Corrsin (18) in a fashion parallel to that of Kolmogorov for the velocity spectrum. Batchelor (19) has given a thorough, lucid treatment of the subject as well as of the spectral limits of applicability and extension into the dissipation range. The basic assumptions in the development of the power density spectrum of homogeneous isotropic temperature fluctuations are listed below.

1. Temperature is a passive quantity; that is, neither the mean temperature nor the temperature fluctuations have any appreciable effect on the velocity structure.

2. The statistical properties of both temperature and velocity in the spectral interval of concern are homogeneous, isotropic, and stationary.

3. With the exception of scaling and dimensionalizing factors, the statistical properties of the temperature fluctuations in the spectral region of interest are determined solely by the velocity field.

4. The concepts of local similarity and cascade of variance apply equally well to temperature as to velocity.

5. The only mechanism for dissipation of thermal variance is molecular conduction, and all of the dissipation occurs in the conduction dissipation range.

6. The Reynolds and Péclet numbers are sufficiently large that an inertial range exists in the velocity spectrum and an intermediate range exists in the temperature power density spectrum where temperature variance is transferred across wavenumbers with no appreciable dissipation by molecular effects. (Batchelor called this intermediate range the convection subrange.)

Corrsin particularized assumption 3 to the postulate that the temperature power density spectrum depends only upon (a) the temperature variance flow rate through the "convective" range and (b) the energy flow rate through the inertial range. The temperature variance flow rate is equal to the total rate of dissipation of temperature variance $D_\theta$,

$$D_\theta = -2\gamma \int_0^\infty k^2\, T(k)dk, \tag{5}$$

with dimensions temperature-squared divided by time. The energy flow rate through the inertial range equals the total viscous energy dissipation rate $\epsilon_0$,

$$\epsilon_0 = -2\nu \int_0^\infty k^2\, V(k)dk, \tag{6}$$

with dimensions length-squared divided by time cubed. The symbols represent the following:

$T$ is temperature power density spectrum,

$$\gamma = \kappa/\overline{\rho} c_p, \tag{7}$$

$\kappa$ is thermal conductivity,

$\overline{\rho}$ is mean density,

$c_p$ is specific heat at constant pressure,

$V$ is velocity spectrum,

$\nu$ is kinematic viscosity.

This postulate restricts the analysis to wavenumbers common to both the inertial and convective ranges.

A dimensional analysis for the spatial power spectrum of the temperature fluctuations in the convective range gives

$$T_C(k) = \beta D_\theta \epsilon_0^{-1/3} k^{-5/3} \tag{8}$$

where $\beta$ is a dimensionless constant and the subscript $C$ identifies the convective range. Corrsin notes that $T_C(k)$ could be determined alternatively if postulate (b) were replaced by the assumption of a dependence on $V_I(k)$ and use were made of the form of the equation for $V_I(k)$. Observations of the temperature convective range described by $T_C$ have been made in the laboratory by Gibson and Schwartz (20) and in the ocean by Grant, Hughes, Vogel, and Moilliet (15), where results extend into the dissipation range.

In a stably stratified ocean, the mean density gradient eliminates the isotropy of velocity fluctuations in the vertical direction. One well-known consequence of this gradient is the presence of internal waves whose influence on the temperature spectrum is felt in a low-wavenumber range between sources and convection. Temperature fluctuations which appear to have been caused by internal waves were seen by McKean (3).

Due to the mean density gradient, one might suspect (as in the case of velocity fluctuations) the existence of a buoyancy range in the temperature spectrum. It is shown in the next section that the buoyant velocity spectrum induces a buoyant temperature spectrum exibiting a -3 power law for an interval of wavenumbers between internal waves and convection. This phenomenon has received little attention, possibly because of the recent surge of interest in the study of internal waves and dissipation. The various spectral ranges of temperature variance are shown in Fig. 2c along with the theoretical and experimental contributors.

## THEORETICAL DEVELOPMENT

The preceding background section suggests the existence of a buoyancy range in the power spectrum of random temperature fluctuations. This section is devoted to the development of the form of the horizontal spatial temperature spectrum in the wavenumber

range between internal waves and conductive dissipation (see Fig. 2b). Dimensional analysis is used to develop the form of the temperature spectrum in the presence of buoyancy forces.

The first step in the theoretical treatment of horizontal spatial temperature fluctuations in a layered medium throughout the buoyancy-convective range consists of a careful review and modification of the assumptions applicable in an isotropic medium. The assumptions listed below apply in the stratified ocean.

1. Temperature is no longer passive. Although the temperature fluctuations are still so small as to have no appreciable effect on the velocity field, the mean temperature gradient, through its effect on density, does directly influence the velocity structure.

1a. The mean density gradient is statically stable.

2. The statistical properties of both temperature and velocity in the spectral range of interest are homogeneous and isotropic only in horizontal planes and are stationary.

3. With the exception of scaling and dimensional factors, the statistical properties of the temperature fluctuations in the spectral range of interest are determined solely by the velocity field.*

4. The concepts of local similarity and cascade of variance apply equally well to temperature as to velocity.

5. The only mechanism for dissipation of thermal variance is molecular conduction, and all of the dissipation occurs in the conduction dissipation range.

6. The Reynolds and Péclet numbers are sufficiently large that a buoyancy-inertial range exists in the velocity spectrum and a spectral range exists where temperature variance is transferred across wavenumbers with no appreciable dissipation. This will be denoted the buoyancy-convective range.

In order to perform a dimensional analysis on the temperature power density spectrum $T_{BC}(k)$ in the buoyancy-convective range, one must particularize assumption 3. It is postulated that $T_{BC}(k)$ depends only upon (a) $D_\theta$, temperature variance flow rate through the buoyancy-convective range; (b) $\epsilon_0$, the total viscous energy dissipation rate; and (c) the form of the velocity spectrum $V_{BI}(k)$ in the buoyancy-inertial range. Since the velocity spectrum in the buoyancy-inertial range is not completely determined by $\epsilon_0$, portions $b$ and $c$ of the postulate are not redundant and interchangeable as they were in Corrsin's analysis of the convective range.

It should be noted that $\nu/\gamma > 1$ in the ocean, and Batchelor (19) has shown that conductive dissipation will begin at a higher wavenumber than viscous dissipation. Thus, the range of validity for the present analysis is the buoyancy-inertial range.

*A similar assumption was made by both Lumley and Phillips in their investigations of buoyancy effects on the velocity spectrum.

The dimensional analysis, based on the above postulate, proceeds in the following manner. Let

$$T_{BC}(k) = G(D_\theta, \epsilon_0, V_{BI}), \tag{9}$$

where $G$ is an unknown universal function of its arguments. By writing the equation as an equality of the dimensions one has

$$\phi^2 \ell = \left(\frac{\phi^2}{t}\right)^h \left(\frac{\ell^2}{t^3}\right)^m \left(\frac{\ell^3}{t^2}\right)^p , \tag{10}$$

where the dimensional units are $\phi$, temperature; $\ell$, length; and $t$, time. The exponents $h$, $m$, and $p$ are to be found so that the equality is satisfied. A set of three simultaneous equations (one for each dimensional unit) can be written from the dimensional equation:

$$\phi: \quad 2 = 2h \tag{11}$$

$$t: \quad 0 = -h - 3m - 2p \tag{12}$$

$$\ell: \quad 1 = 2m + 3p. \tag{13}$$

Solving the set of simultaneous equations gives as the solution,

$$h = 1, \quad m = -1, \quad p = 1. \tag{14}$$

Thus

$$T_{BC}(k) = B\, D_\theta\, \epsilon_0^{-1}\, \epsilon^{2/3}\, k^{-5/3}, \tag{15}$$

where $B$ is a dimensionless constant and the form of the velocity spectrum in the buoyancy-inertial range has been utilized. Substitution for $\epsilon$ from Eq. (3) in the above equation gives

$$T_{BC}(k) = B\, D_\theta\, \epsilon_0^{-1/3} \left[1 + \left(\frac{k_b}{k}\right)^{4/3}\right] k^{-5/3} \tag{16}$$

With $T_{BC}$ written in the form of Eq. (16), it is obvious that for $k >> k_b$ (i.e., $k$ in the convective range) $T_{BC}$ reduces to $T_C$ as would be expected. Using the definition of $k_b$ (Eq. (4)) in Eq. (16) gives

$$T_{BC}(k) = B\, D_\theta\, \epsilon_0^{-1/3}\, k^{-5/3} + BCD_\theta N^2 \epsilon_0^{-1}\, k^{-3}, \tag{17}$$

which can be rewritten as

$$T_{BC}(k) = A_1 k^{-5/3} + A_2 k^{-3}, \tag{18}$$

where

$$A_1 = BD_\theta \epsilon_0^{-1/3} \tag{19}$$

$$A_2 = BCD_\theta N^2 \epsilon_0^{-1}. \tag{20}$$

Based on the notationally simple form of $T_{BC}$ in Eq. (18), one can give an explanation of temperature power spectral laws varying between -5/3 and -3.

If one chooses to analyze an intermediate wavenumber range, a power law between -3 and -5/3 will result. As the analysis range is extended into the larger wavenumbers, convection begins to dominate and the power law approaches -5/3. On the other hand, as smaller wavenumbers are included in the analysis, the buoyancy effects are felt and the power law tends to -3.

Another aspect related to the power law determination concerns a physical property of a density-stratified fluid, the Brunt-Vaisala frequency $N$. The ratio of the two coefficients $A_1$ and $A_2$ in Eq. (18) and consequently, the relative importance of the -3 and -5/3 power laws, is a function of $N$. Therefore, in a fixed $k$-range, one can observe power laws between -3 and -5/3 due strictly to physical causes. For example, see Fig. 3 where the transition wavenumbers $k_b$ and $k_b'$ (above which inertial turbulence is the dominant influence) correspond to large and small values of $N$, respectively. When the Brunt-Väisälä frequency is large, the ratio $A_2/A_1$ is also large, and consequently the -3 region expands. Power law analysis in the fixed interval $k_L - k_U$ for the two curves in Fig. 3 will yield considerably different results.

Once $A_1$, $A_2$, and $N$ have been determined, they can be manipulated to form estimates of $\epsilon_0$ and $D_\theta$ using the fact that the constants $B$ and $C$ are of order unity (18). From Eqs. (19) and (20), one can form the quantity

$$\frac{A_2}{A_1 N^2} = \frac{(BCD_\theta N^2 \epsilon_0^{-1})}{(BD_\theta \epsilon_0^{-1/3}) N^2} = \frac{C}{\epsilon_0^{2/3}} \tag{21}$$

so that

$$\epsilon_0 = \left(\frac{A_1 C N^2}{A_2}\right)^{3/2} \approx \left(\frac{A_1 N^2}{A_2}\right)^{3/2} \tag{22}$$

Similarly, one has

$$\frac{A_1^3 N^2}{A_2} = \frac{(BD_\theta \epsilon_0^{-1/3})^3 N^2}{(BCD_\theta N^2 \epsilon_0^{-1})} = \frac{B^2 D_\theta^2}{C} \tag{23}$$

so that

$$D_\theta = \left(\frac{A_1^3 C N^2}{A_2 B^2}\right)^{1/2} \approx \left(\frac{A_1^3 N^2}{A_2}\right)^{1/2} \tag{24}$$

It is interesting that one need not go through velocity spectrum calculations to arrive at an estimate of the total rate of viscous energy dissipation $\epsilon_0$.

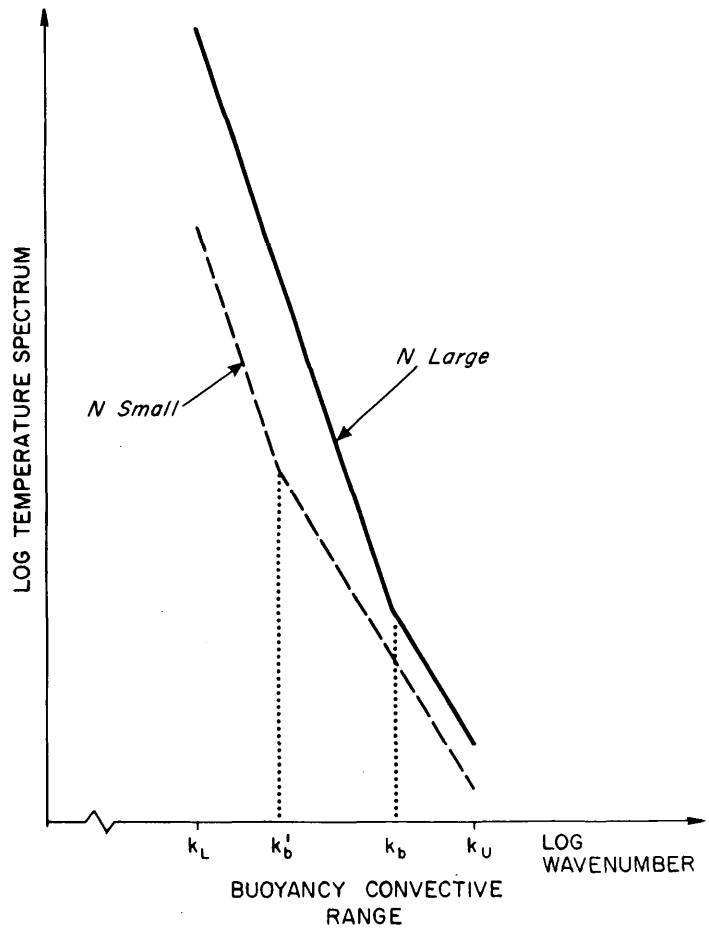


Fig. 3—Temperature power density spectrum in buoyancy-convective range showing effect of Brunt-Väisälä frequency.

In summary, this development shows a two-term power law for temperature fluctuations in the buoyancy-convective range of wavenumbers. The spectral decay associated with buoyancy is shown to be proportional to $k^{-3}$. Contributors to the development of the velocity and temperature spectra in the intermediate wavenumber range are shown in Table 1 for completeness.

Table 1
Contributors to the Development of the Velocity and Temperature Spectra in a Wavenumber Range Between Internal Waves and Dissipation

| Wavenumber Range | Formulation | Contributor |
|---|---|---|
| Inertial | $V_I(k) = \alpha\epsilon_0^{2/3}k^{-5/3}$ | Kolmogorov |
| Buoyancy-Inertial | $V_{BI}(k) = \alpha\epsilon_0^{2/3}k^{-5/3} + \alpha CN^2k^{-3}$ | Lumley |
| Convective | $T_C(k) = \beta D_\theta\epsilon_0^{-1/3}k^{-5/3}$ | Corrsin |
| Buoyancy-Convective | $T_{BC}(k) = BD_\theta\epsilon_0^{-1/3}k^{-5/3} + BCN^2D_\theta\epsilon_0^{-1}k^{-3}$ | Moseley & Del Balzo |

## DATA ANALYSIS

If one were to conduct a temperature microstructure experiment in the open ocean at a variety of depths, one should find a buoyancy-convective range of wavenumbers where (a) power laws span the interval [- 3, - 5/3]; (b) the Brunt-Väiälä frequency has a strong influence on the form of the temperature spectrum; and (c) power laws tend asymptotically toward -3 for increasing $N$. If one's observation interval extends sufficiently far into the convective range, a -5/3 region will be clearly evident. A least-squares analysis in the convective range on the equation $T_C = pk^q$ can be performed, where $p$ will be an estimate of $A_1$ and $q$ will be $\approx$ -5/3. In order to "see" the buoyancy effects, one could next subtract the convective portion of the spectrum throughout the entire buoyancy-convective range. Then, a least-squares analysis on $T_{BC} - pk^q = rk^s$ would yield $r$, which is an estimate of $A_2$, and $s$ which will be $\approx$ -3. At this point, one could obtain estimates of $\epsilon_0$ and $D_\theta$ by using $p$, $r$, and $N$ via Eqs. (22) and (24).

The temperature spectra presented in Appendix B were obtained from horizontally sampled temperature data taken during the open ocean experiment described in Appendix A. The least-squares method was used to fit these spectra according to the power law formulation $T_{BC}(k) = ak^b$, for $k_L < k < k_U$. The lower end of the wavenumber range $k_L$ is set by the spatial transform length, while the upper end $k_U$ is limited to that region for which the squared coherency spectrum* is less than 0.2. This judgement was made to minimize depth-related pseudotemperatures which can not be fully removed due to medium instability and nonlinear temperature-depth correlations. Some further analysis along these lines is presented in Appendix C. Although limited by ship movement at swell frequencies, $k_U$ is large enough to permit analysis in the buoyancy-convective range.

The method of least squares, should not be applied directly to the equation $T_{BC}(k) = ak^b$, since $T_{BC}$ has a variance which is proportional to its mean. However, on a logarithmic scale the confidence interval about $T_{BC}(k)$ is constant with wavenumber. Therefore the proper equation to least squares fit is $\log [T_{BC}(k)] = \log a + b \log k$. This fit yields unbiased estimates of $\log a$ and $b$.

The results of this least-squares analysis are presented in Fig. 4 and in Table 2, where $b$ is the power law and $a$ is the power intercept. As predicted, $b$ varies between -3 and -5/3. The power law as a function of depth strongly suggests a dependence of $b$ on $N$, the Brunt-Väisälä frequency. This is no surprise due to the form of $T_{BC}$ in Eq. (17);

$$T_{BC}(k) = BD_\theta \epsilon_0^{-1/3} k^{-5/3} + BCD_\theta N^2 \epsilon_0^{-1} k^{-3}. \tag{17}$$

There also appears to be an asymptotic dependence of $b$ on $G_T$ (temperature gradient); i.e., $b \rightarrow -3$ for very large $G_T$. Again, this is anticipated from the form of Eq. (17) since $G_T$ is proportional to $N^2$. These relationships will be discussed in greater detail in the coefficient study section.

*See Appendix A

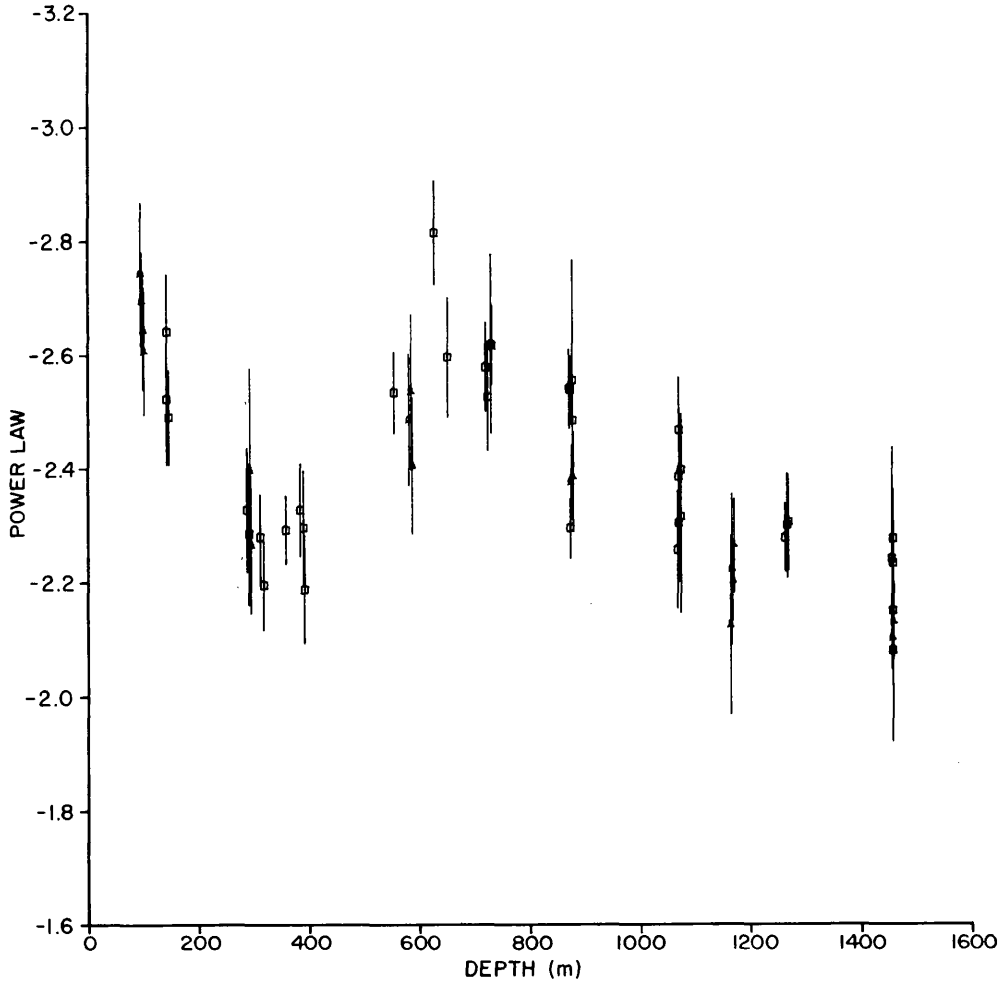


(a)

Fig. 4—Least-squares results with 90% confidence limits (□ = Station 1, △ = Station 2), for (a) power law vs depth, (b) power law vs negative temperature gradient, (c) power intercept vs depth, and (d) power intercept vs negative temperature gradient.

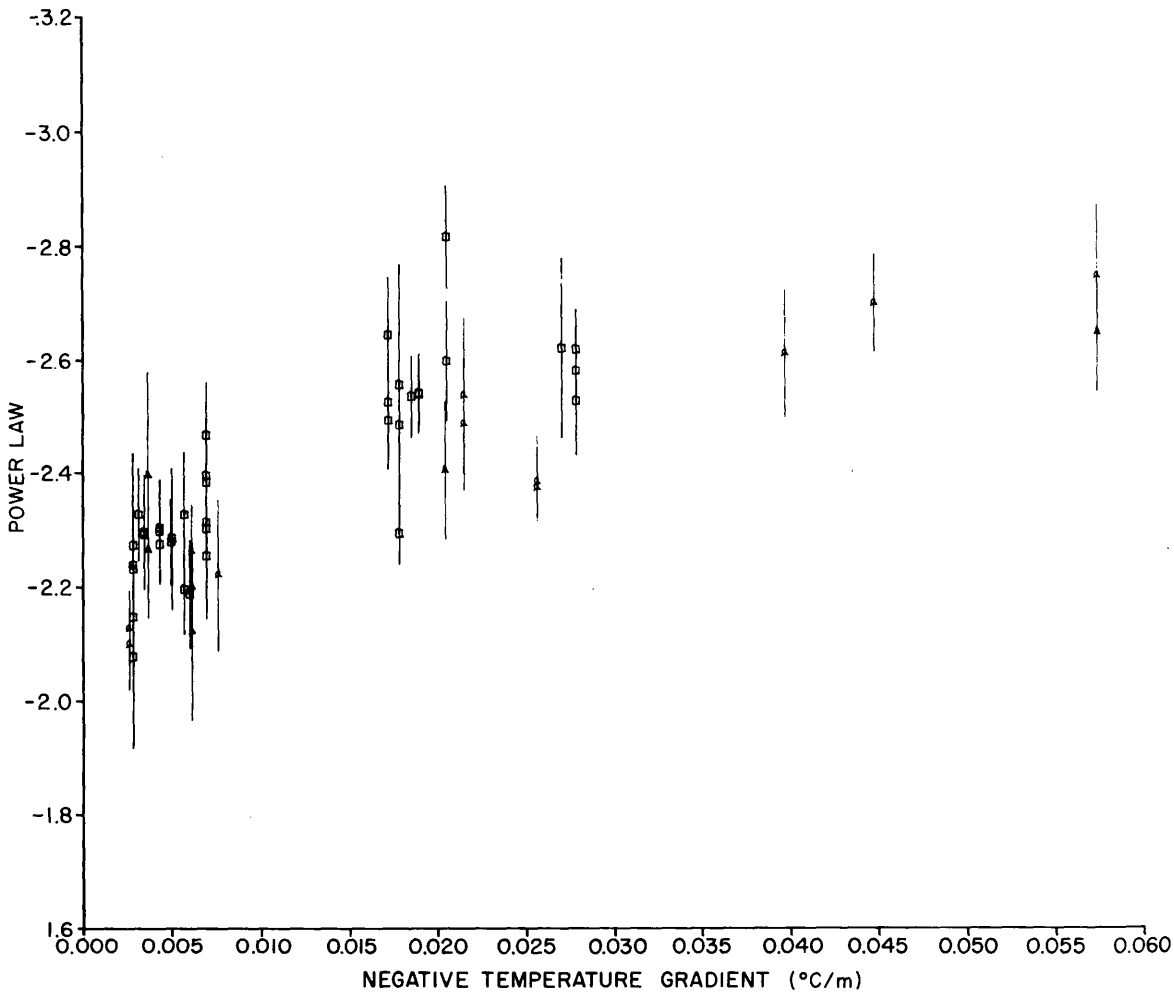


(b)

Fig. 4—Least-squares results with 90% confidence limits (□ = Station 1, △ = Station 2), for (a) power law vs depth, (b) power law vs negative temperature gradient, (c) power intercept vs depth, and (d) power intercept vs negative temperature gradient. (Continued)

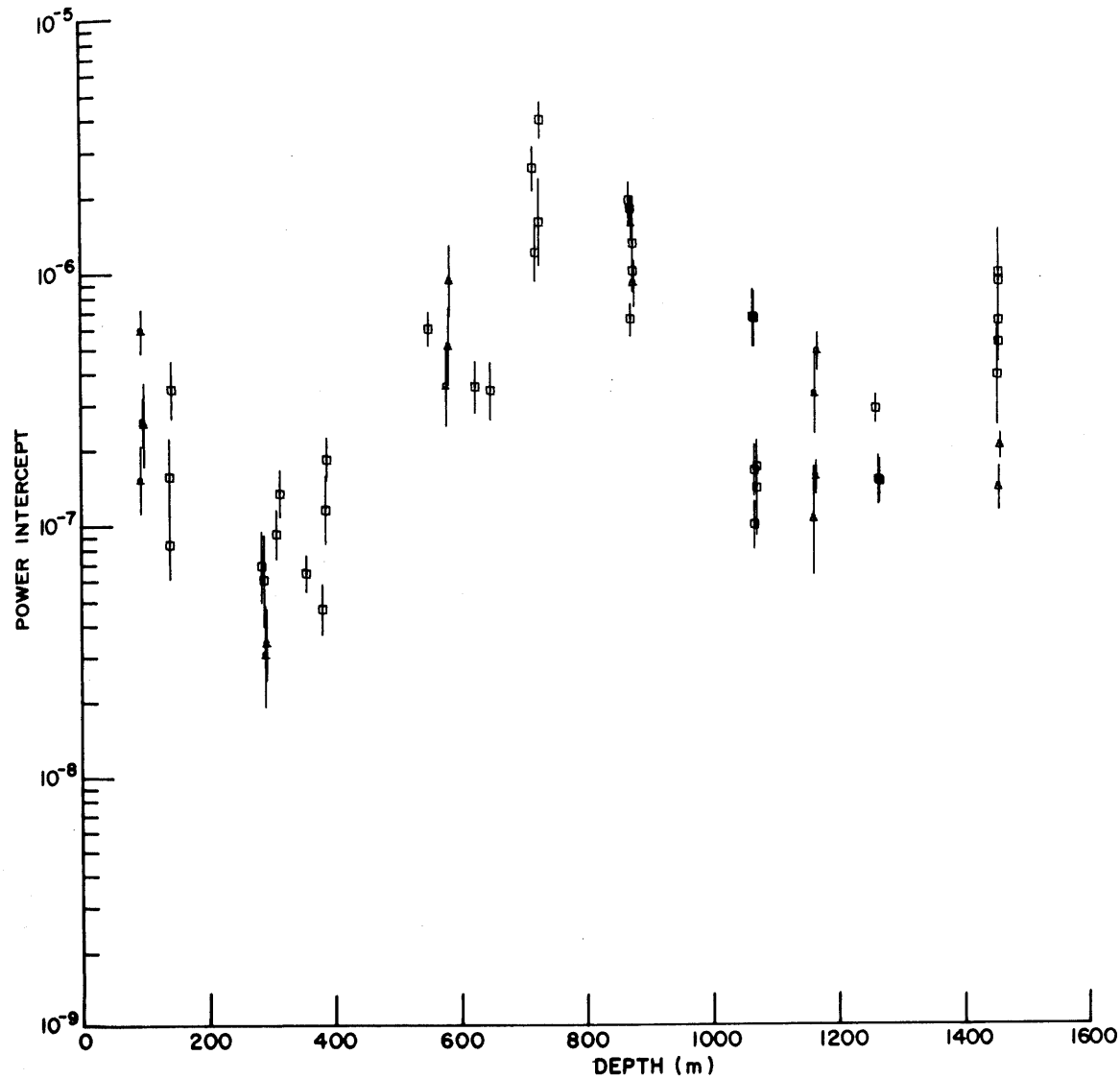


(c)

Fig. 4—Least-squares results with 90% confidence limits (□ = Station 1, △ = Station 2), for (a) power law vs depth, (b) power law vs negative temperature gradient, (c) power intercept vs depth, and (d) power intercept vs negative temperature gradient. (Continued)

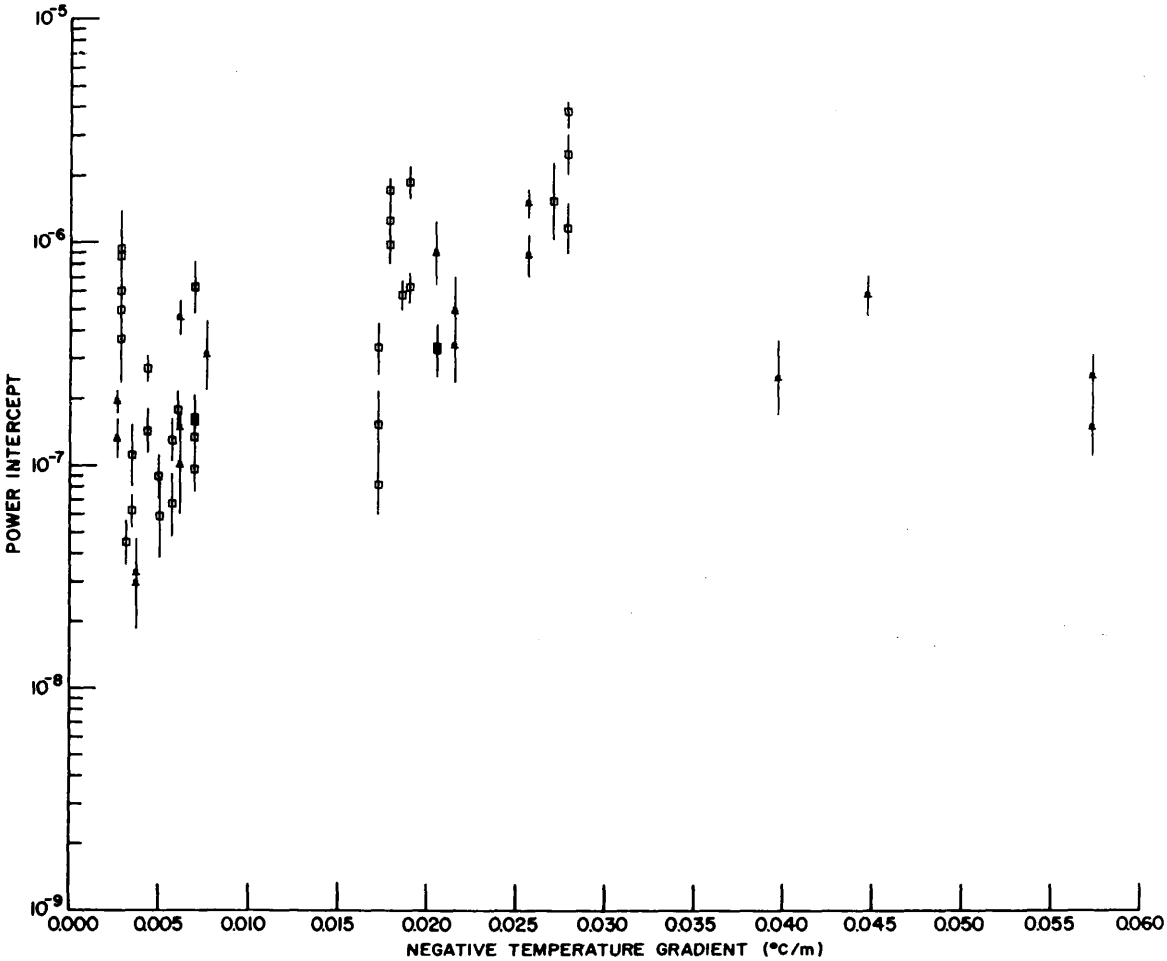


(d)

Fig. 4—Least-squares results with 90% confidence limits (□ = Station 1, △ = Station 2), for (a) power law vs depth, (b) power law vs negative temperature gradient, (c) power intercept vs depth, and (d) power intercept vs negative temperature gradient. (Continued)

Table 2
Least Squares Analysis on $T_{BC} = ak^b$
Throughout the Observed Buoyancy—Convective Range ($k_L - k_U$)

| Run | $k_L \times 10^2$ ($m^{-1}$) | $k_U \times 10^2$ ($m^{-1}$) | $a \times 10^8$ | 90% Confidence Limits on $a \times 10^8$ | | $b$ | 90% Confidence Limits on $b$ | |
|---|---|---|---|---|---|---|---|---|
| 1-150-1 | 0.63 | 14.75 | 8.2 | 6.1 | 10.9 | -2.64 | -2.74 | -2.54 |
| 1-150-2 | 0.64 | 12.09 | 33.6 | 26.0 | 43.4 | -2.49 | -2.57 | -2.41 |
| 1-150-3 | 0.65 | 11.71 | 15.2 | 10.7 | 21.7 | -2.52 | -2.64 | -2.41 |
| 1-300-1 | 0.65 | 8.81 | 5.9 | 3.9 | 8.9 | -2.29 | -2.41 | -2.16 |
| 1-300-2 | 0.63 | 13.46 | 6.7 | 4.9 | 9.2 | -2.33 | -2.43 | -2.22 |
| 1-300-3 | 0.71 | 16.60 | 13.1 | 10.5 | 16.2 | -2.20 | -2.27 | -2.12 |
| 1-300-4 | 0.68 | 14.51 | 9.0 | 7.2 | 11.2 | -2.28 | -2.35 | -2.20 |
| 1-400-1 | 0.73 | 11.33 | 11.1 | 8.2 | 15.2 | -2.30 | -2.40 | -2.20 |
| 1-400-2 | 0.65 | 18.69 | 6.3 | 5.4 | 7.4 | -2.29 | -2.35 | -2.23 |
| 1-400-3 | 0.71 | 15.59 | 4.5 | 3.6 | 5.7 | -2.33 | -2.41 | -2.25 |
| 1-400-4 | 1.31 | 38.52 | 17.8 | 14.8 | 21.5 | -2.19 | -2.28 | -2.09 |
| 1-550-2 | 1.41 | 19.04 | 34.2 | 27.2 | 43.0 | -2.81 | -2.90 | -2.72 |
| 1-550-3 | 1.45 | 21.79 | 32.9 | 25.5 | 42.5 | -2.60 | -2.70 | -2.50 |
| 1-550-4 | 1.62 | 33.97 | 57.8 | 49.8 | 67.1 | -2.53 | -2.60 | -2.46 |
| 1-750-1 | 0.97 | 17.53 | 116.1 | 90.1 | 149.4 | -2.53 | -2.62 | -2.43 |
| 1-750-2 | 1.24 | 20.50 | 247.2 | 203.6 | 300.2 | -2.58 | -2.65 | -2.50 |
| 1-750-3 | 1.28 | 23.73 | 383.4 | 325.0 | 452.2 | -2.62 | -2.69 | -2.55 |
| 1-750-4 | 3.68 | 14.73 | 153.1 | 103.8 | 225.9 | -2.62 | -2.77 | -2.46 |
| 1-900-1 | 1.23 | 25.15 | 184.8 | 157.3 | 217.2 | -2.54 | -2.61 | -2.47 |
| 1-900-2 | 1.28 | 21.20 | 62.7 | 54.3 | 72.5 | -2.54 | -2.60 | -2.48 |
| 1-900-3 | 1.14 | 33.74 | 96.9 | 85.5 | 110.0 | -2.48 | -2.54 | -2.43 |
| 1-900-4 | 6.63 | 22.10 | 125.3 | 81.5 | 192.6 | -2.55 | -2.76 | -2.34 |
| 1-900-5 | 1.29 | 28.38 | 172.2 | 153.6 | 193.1 | -2.29 | -2.34 | -2.24 |
| 1-900-6 | 1.01 | 10.65 | 340.0 | 166.1 | 696.1 | -2.26 | -2.49 | -2.03 |
| 1-1100-1 | 1.58 | 27.56 | 9.6 | 7.8 | 11.9 | -2.47 | -2.56 | -2.38 |
| 1-1100-2 | 1.20 | 35.36 | 62.8 | 49.1 | 80.4 | -2.38 | -2.50 | -2.26 |
| 1-1100-4 | 1.39 | 36.73 | 15.7 | 12.5 | 19.8 | -2.30 | -2.40 | -2.20 |
| 1-1100-5 | 1.07 | 20.41 | 13.5 | 8.8 | 20.7 | -2.31 | -2.48 | -2.15 |
| 1-1100-6 | 0.98 | 30.00 | 16.3 | 13.0 | 20.5 | -2.40 | -2.49 | -2.30 |
| 1-1100-7 | 0.99 | 21.23 | 63.3 | 48.9 | 82.0 | -2.25 | -2.36 | -2.15 |
| 1-1300-1 | 1.13 | 25.46 | 14.3 | 11.7 | 17.3 | -2.30 | -2.38 | -2.22 |
| 1-1300-2 | 1.14 | 36.56 | 27.5 | 24.3 | 31.0 | -2.28 | -2.33 | -2.22 |
| 1-1300-3 | 1.04 | 23.40 | 14.4 | 11.5 | 18.0 | -2.30 | -2.39 | -2.21 |
| 1-1500-1 | 1.79 | 48.44 | 86.9 | 76.6 | 98.6 | -2.15 | -2.22 | -2.08 |
| 1-1500-2 | 1.12 | 22.48 | 93.6 | 63.1 | 139.0 | -2.08 | -2.24 | -1.92 |
| 1-1500-3 | 1.57 | 25.96 | 37.1 | 23.7 | 58.0 | -2.24 | -2.43 | -2.05 |
| 1-1500-4 | 1.38 | 35.77 | 50.0 | 41.9 | 59.7 | -2.27 | -2.36 | -2.19 |
| 1-1500-5 | 1.40 | 26.59 | 60.7 | 51.7 | 71.4 | -2.23 | -2.30 | -2.16 |
| 2-100-1 | 1.28 | 22.96 | 14.8 | 10.9 | 20.0 | -2.74 | -2.87 | -2.62 |
| 2-100-2 | 1.28 | 6.39 | 24.6 | 17.0 | 35.7 | -2.61 | -2.72 | -2.50 |
| 2-100-3 | 1.36 | 27.29 | 57.6 | 47.4 | 70.0 | -2.70 | -2.78 | -2.61 |
| 2-100-4 | 1.46 | 30.62 | 25.1 | 20.0 | 31.3 | -2.64 | -2.75 | -2.54 |
| 2-300-1 | 1.61 | 22.59 | 3.0 | 1.9 | 4.7 | -2.40 | -2.58 | -2.22 |
| 2-300-2 | 1.21 | 17.49 | 3.3 | 2.4 | 4.6 | -2.27 | -2.39 | -2.15 |
| 2-600-1 | 1.21 | 9.10 | 34.3 | 23.9 | 49.5 | -2.49 | -2.60 | -2.37 |
| 2-600-2 | 1.57 | 18.09 | 49.4 | 34.8 | 70.1 | -2.54 | -2.67 | -2.40 |
| 2-600-3 | 1.51 | 15.81 | 89.9 | 65.0 | 124.3 | -2.41 | -2.53 | -2.29 |
| 2-900-1 | 1.12 | 33.11 | 149.2 | 129.7 | 171.7 | -2.37 | -2.44 | -2.31 |
| 2-900-2 | 1.30 | 18.17 | 86.9 | 70.5 | 107.0 | -2.38 | -2.46 | -2.30 |
| 2-1200-1 | 1.44 | 34.53 | 46.3 | 39.1 | 55.0 | -2.26 | -2.35 | -2.18 |
| 2-1200-2 | 1.25 | 8.73 | 10.0 | 6.2 | 16.4 | -2.12 | -2.29 | -1.97 |
| 2-1200-3 | 1.21 | 17.54 | 31.3 | 22.0 | 44.4 | -2.22 | -2.35 | -2.09 |
| 2-1200-4 | 1.11 | 33.16 | 14.8 | 12.7 | 17.2 | -2.20 | -2.27 | -2.13 |
| 2-1500-1 | 1.34 | 20.13 | 13.3 | 10.9 | 16.2 | -2.10 | -2.18 | -2.02 |
| 2-1500-2 | 1.42 | 50.40 | 19.4 | 17.3 | 21.8 | -2.13 | -2.19 | -2.06 |

## COEFFICIENT STUDY

A visual analysis of the power spectrum plots in Appendix B shows 19 runs with a noticeable -5/3 region. These were chosen for further analysis in an effort to determine the coefficients in Eq. (18) and estimate $\epsilon_0$, the total viscous energy dissipation rate, and $D_\theta$, the total temperature variance dissipation rate.

Each of the 19 runs was least-squares fit in the convective range according to the equation $T_C(k) = pk^q$. The results are given in Table 3.* The mean value of $q$ is -1.68. As anticipated from both the theory and visual analysis, $q$ is essentially identical to the classical -5/3 value.

Table 3
Least Squares Analysis on $T_C = pk^q$ in the Convective Range ($k_L$ - $k_U$)

| Run | $k_L \times 10^2$ ($m^{-1}$) | $k_U \times 10^2$ ($m^{-1}$) | $p \times 10^7$ | 90% Confidence Limits on $p \times 10^7$ | | $q$ | 90% Confidence Limits on $q$ | |
|---|---|---|---|---|---|---|---|---|
| 1-150-1 | 6.91 | 14.12 | 5.8 | 1.9 | 17.5 | -1.75 | -2.24 | -1.26 |
| 1-150-2 | 11.45 | 18.45 | 20.9 | 6.5 | 67.1 | -1.64 | -2.25 | -1.03 |
| 1-300-1 | 5.55 | 15.98 | 3.0 | 1.6 | 5.8 | -1.67 | -1.95 | -1.40 |
| 1-400-2 | 5.80 | 13.21 | 2.7 | 1.5 | 5.0 | -1.69 | -1.94 | -1.44 |
| 1-550-2 | 21.86 | 31.02 | 12.8 | 5.4 | 30.6 | -1.75 | -2.40 | -1.10 |
| 1-550-3 | 10.17 | 39.23 | 19.4 | 15.4 | 24.4 | -1.66 | -1.81 | -1.51 |
| 1-750-1 | 8.28 | 24.84 | 68.8 | 42.8 | 110.6 | -1.67 | -1.93 | -1.42 |
| 1-750-4 | 12.89 | 23.32 | 95.4 | 52.7 | 172.8 | -1.68 | -2.02 | -1.33 |
| 1-900-4 | 15.47 | 27.62 | 48.8 | 20.5 | 116.0 | -1.71 | -2.27 | -1.16 |
| 1-900-5 | 21.93 | 46.44 | 37.2 | 29.8 | 46.5 | -1.69 | -1.89 | -1.49 |
| 1-900-6 | 11.16 | 26.37 | 118.4 | 75.0 | 187.2 | -1.70 | -1.96 | -1.43 |
| 1-1100-7 | 5.43 | 16.29 | 20.9 | 10.9 | 40.1 | -1.72 | -2.00 | -1.43 |
| 2-100-3 | 14.33 | 39.57 | 31.4 | 26.3 | 37.6 | -1.65 | -1.78 | -1.53 |
| 2-100-4 | 14.58 | 32.07 | 10.3 | 6.1 | 17.5 | -1.66 | -2.02 | -1.31 |
| 2-600-1 | 18.20 | 27.30 | 14.8 | 7.1 | 30.6 | -1.71 | -2.20 | -1.22 |
| 2-600-2 | 14.95 | 35.40 | 20.0 | 14.9 | 27.0 | -1.67 | -1.88 | -1.46 |
| 2-900-2 | 16.87 | 35.69 | 25.1 | 17.6 | 35.8 | -1.72 | -1.98 | -1.46 |
| 2-1200-2 | 8.73 | 24.95 | 3.1 | 1.9 | 5.2 | -1.64 | -1.91 | -1.37 |
| 2-1200-4 | 13.82 | 33.16 | 3.0 | 2.1 | 4.3 | -1.69 | -1.94 | -1.45 |

*Note the relation between the convective range and the Brunt-Väisälä frequency. When $N$ is large (see Fig. 3), the convective $k$-range falls in higher wavenumbers than when $N$ is small.

To determine the power law in the buoyancy range, a least-squares analysis is performed over the entire observed buoyancy-convective range on the equation $T_{BC} - pk^q = rk^s$, with $p$ and $q$ as determined in the convective range.* The results, presented in Table 4† show the mean value of $s$ to be -2.94, very close to the predicted -3. In fact, 12 of the 19 individual runs have 90% confidence limits which include -3. The distribution of $s$ values, as a function of $q$ for the same run is presented in Fig. 5 and no noticeable trend is observed. Also shown are the one standard deviation ($1\sigma$) bounds on the $s$-distribution and the 90% confidence limits on the mean of the $s$-distribution‡ which includes the value -3. Thus, we conclude that the mean is not significantly different from -3.

Table 4
Least Squares Analysis on $T_{BC} - pk^q = rk^s$ through the Buoyancy—Convective Range ($k_L - k_U$)

| Run | $k_L \times 10^2$ ($m^{-1}$) | $k_U \times 10^2$ ($m^{-1}$) | $r \times 10^9$ | 90% Confidence Limits on $r \times 10^9$ | | $s$ | 90% Confidence Limits on $s$ | |
|---|---|---|---|---|---|---|---|---|
| 1-150-1 | 0.63 | 14.12 | 7.8 | 3.5 | 17.2 | -3.16 | -3.40 | -2.91 |
| 1-150-2 | 0.64 | 18.45 | 24.9 | 13.0 | 47.8 | -3.07 | -3.29 | -2.85 |
| 1-300-1 | 0.65 | 15.98 | 17.3 | 8.4 | 35.8 | -2.44 | -2.65 | -2.24 |
| 1-400-2 | 1.93 | 13.21 | 3.4 | 1.0 | 11.8 | -2.93 | -3.33 | -2.52 |
| 1-550-2 | 1.41 | 31.02 | 46.2 | 29.3 | 72.9 | -3.39 | -3.58 | -3.20 |
| 1-550-3 | 1.45 | 39.23 | 140.7 | 70.1 | 282.4 | -2.69 | -2.97 | -2.41 |
| 1-750-1 | 0.97 | 24.84 | 72.1 | 19.5 | 266.9 | -3.09 | -3.57 | -2.60 |
| 1-750-4 | 1.23 | 23.32 | 166.3 | 80.4 | 343.8 | -3.06 | -3.33 | -2.79 |
| 1-900-4 | 1.10 | 27.62 | 143.9 | 75.8 | 273.0 | -3.15 | -3.41 | -2.89 |
| 1-900-5 | 1.29 | 36.44 | 208.2 | 162.3 | 266.9 | -2.81 | -2.92 | -2.70 |
| 1-900-6 | 2.03 | 26.37 | 264.7 | 97.8 | 716.2 | -2.76 | -3.17 | -2.39 |
| 1-1100-7 | 0.99 | 16.29 | 27.9 | 5.2 | 149.0 | -2.84 | -3.41 | -2.28 |
| 2-100-3 | 1.36 | 39.57 | 42.4 | 24.3 | 74.1 | -3.37 | -3.60 | -3.14 |
| 2-100-4 | 1.46 | 32.07 | 63.4 | 35.6 | 112.9 | -3.01 | -3.23 | -2.78 |
| 2-600-1 | 2.43 | 27.30 | 101.6 | 59.5 | 173.7 | -2.74 | -2.96 | -2.52 |
| 2-600-2 | 1.57 | 35.40 | 48.4 | 27.5 | 85.5 | -3.16 | -3.40 | -2.92 |
| 2-900-2 | 1.95 | 35.69 | 71.2 | 41.6 | 122.0 | -3.01 | -3.25 | -2.78 |
| 2-1200-2 | 1.25 | 24.95 | 18.2 | 7.5 | 44.4 | -2.35 | -2.64 | -2.05 |
| 2-1200-4 | 1.11 | 33.16 | 30.2 | 13.1 | 69.6 | -2.52 | -2.82 | -2.23 |

*In this analysis, $pk^q$ is considered similar to a noise level and only those data which are a predetermined, fixed amount greater than $pk^q$ are retained in the least-squares analysis.
†Again, the $k$-range of interest varies with $N$.
‡The assumption is made that the $s$ values are distributed normally about the mean, and use is made of Student's $t$-distribution.

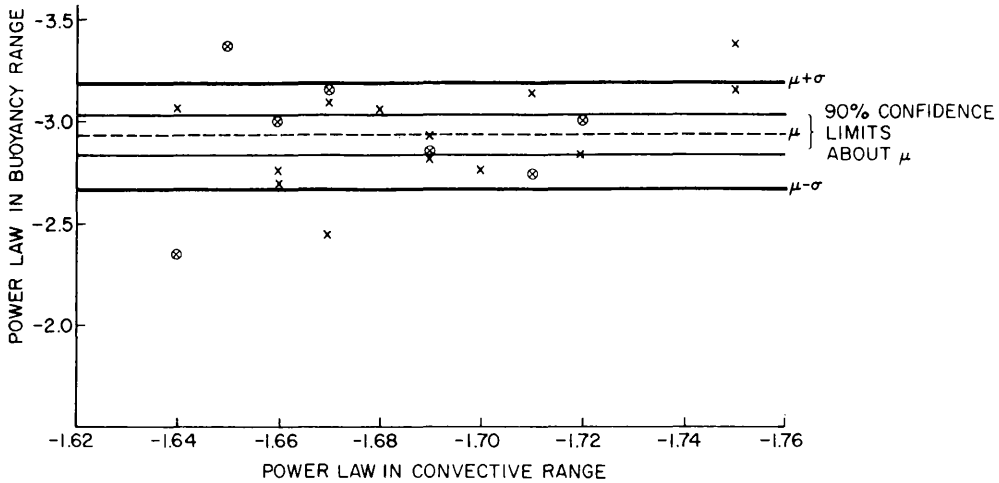


Fig. 5—Least-squares analysis on power laws in buoyancy and convective ranges with distribution mean $\mu$ and $1\sigma$

Since the theory indicates that $q$ and $s$ should equal -5/3 and -3, respectively, another type of analysis is suggested. Perform the least-squares fits over the same regions but force the theoretically predicted power laws and ascertain estimates of $A_1$ and $A_2$. The equations $T_C = p'k^{-5/3}$ and $T_{BC} - p'k^{-5/3} = r'k^{-3}$ (using $p'$ as calculated in the first equation) are fit in the identical $k$-ranges as before and the values are plotted vs depth in Figs. 6 and 7. The solid line was faired in by eye. The similarity to the shape of the Brunt-Väisälä frequency profile is unmistakable.

One further area of analysis concerns the physical parameters $\epsilon_0$ and $D_\theta$. Using the estimates $p'$ and $r'$ of the coefficients $A_1$ and $A_2$, respectively, together with the run-by-run values of $N$ for each tow, the quantities $\epsilon_0 C^{-3/2}$ and $BD_\theta C^{-1/2}$ are calculated via Eqs. (22) and (24). The constants $B$ and $C$ are of order unity (18) and they are set equal to one in order to estimate $\epsilon_0$ and $D_\theta$ directly. The results are presented graphically in Figs. 8 and 9. Again, note the apparent influence of the Brunt-Väisälä frequency. Webster (16) predicted and verified experimentally a proportionality between the rate of energy dissipation and $N$. Grant, Stewart, and Moilliet (14) have experimental evidence of energy dissipation rates $\epsilon_0$ between $1.02 \times 10^{-4}$ and $1.5 \times 10^{-7}$ $m^2/s^3$. Our data show a range of values between $2.0 \times 10^{-4}$ and $3.2 \times 10^{-6}$ $m^2/s^3$ which agrees well with the values seen by Grant, et al.

Numerous combinations of parameters were least-squares fit and the results are given in Table 5 for completeness.

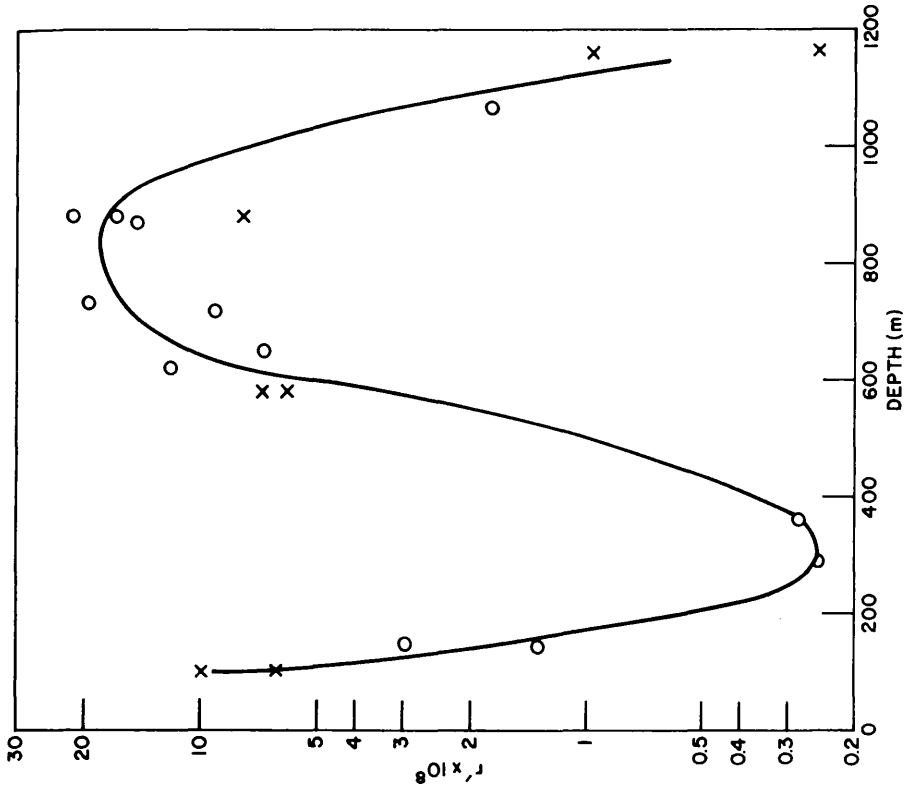


Fig. 7—Least-squares analysis on $T_{BC}(k) - p'k^{-5/3} = r'k^{-3}$
(0 = Station 1, $x$ = Station 2)

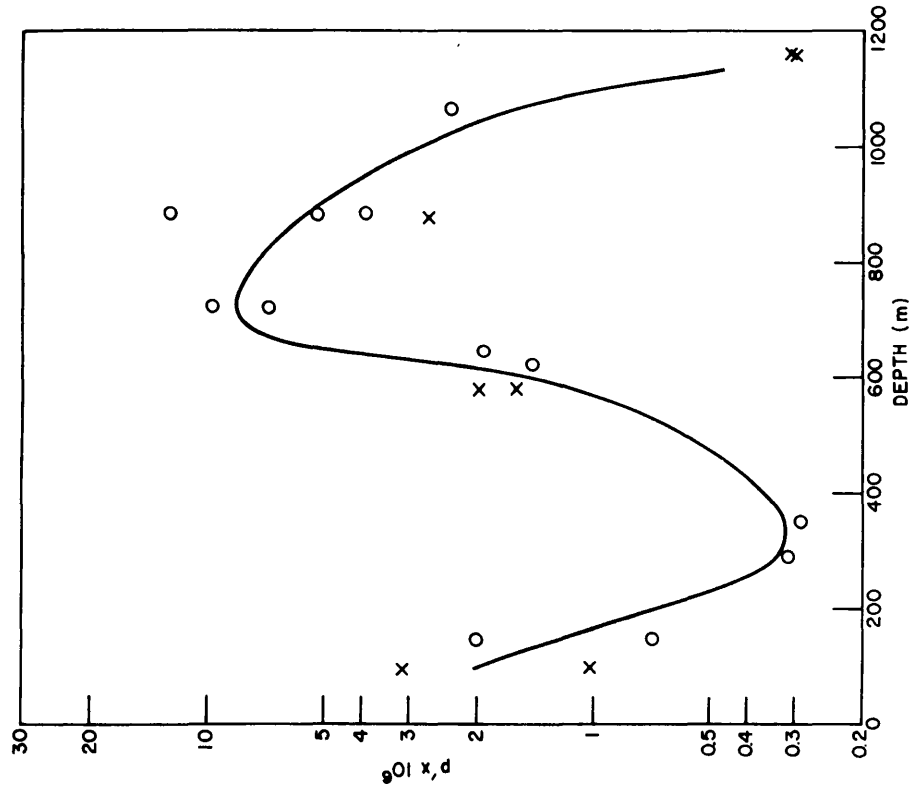


Fig. 6—Least-squares analysis on $T_C(k) = p'k^{-5/3}$
(0 = Station 1, $x$ = Station 2)

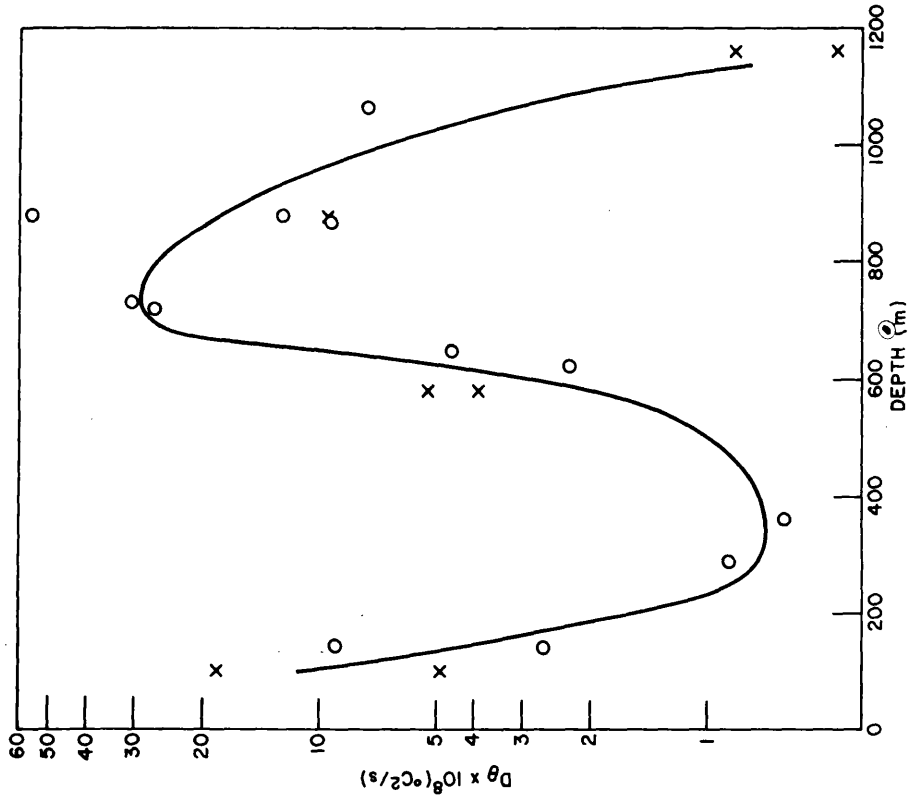


Fig. 9—Total rate of dissipation of temperature variance (0 = Station 1, $x$ = Station 2)

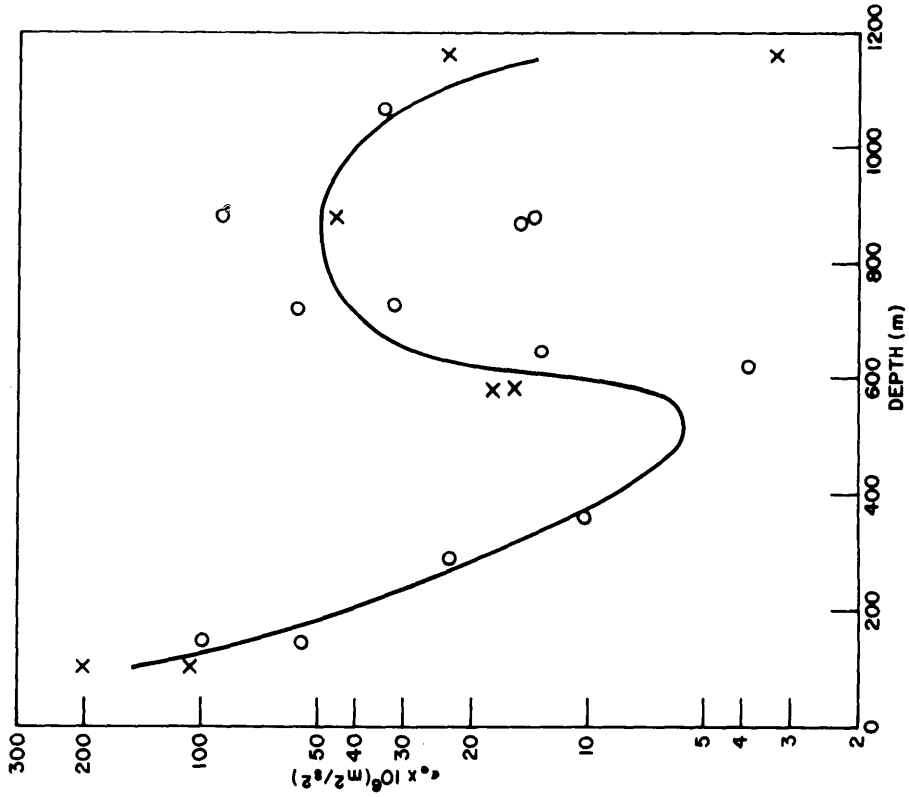


Fig. 8—Total rate of energy dissipation vs depth (0 = Station 1, $x$ = Station 2)

Table 5.
Least-squares Relationships to the Brunt-Väisälä Frequency

| Equation | Results (MKS System) | |
|---|---|---|
| $p' = u_1 N^{v1}$ | $u_1 = 1.45 \times 10^{-3}$ | $v_1 = 1.24$ |
| $r' = u_2 N^{v2}$ | $u_2 = 5.98 \times 10^{-3}$ | $v_2 = 2.21$ |
| $\epsilon_0 C^{-3/2} = u_3 N^{v3}$ | $u_3 = 1.19 \times 10^{-1}$ | $v_3 = 1.55$ |
| $BD_\theta\ C^{-1/2} = u_4 N^{v4}$ | $u_4 = 6.46 \times 10^{-4}$ | $v_4 = 1.75$ |

## AN OVERVIEW OF OCEANIC TEMPERATURE FLUCTUATIONS

The spatial spectrum of horizontal temperature fluctuations in a stratified ocean may be divided into several regions as shown in Fig. 10. The lowest wavenumber range is likely to be dominated by large-scale, weather-related thermal activity and ocean currents. The underlying dynamic mechanism in the next higher wavenumber range is estimated to be internal waves. At the high end of this range, the spectrum decays as $k^{-2}$ due to a modulation of the sheet and layer structure by the internal wave field, as developed by Phillips (21). This effect is predicted (22) to extend beyond the Brunt-Väisälä wavenumber cutoff. Experimental evidence of a -2 power law is given by McKean (3). At larger wavenumbers, one finds the buoyancy and convective ranges with -3 and -5/3 power laws, respectively, that were treated in this report. Finally, the dissipative range lies in the highest wavenumber interval. Batchelor (19) predicted that the spectrum between the viscous and conductive cut-off wavenumbers is proportional to $k^{-1}$ and this was seen by Grant, et al (15). Above the conductive cutoff the spectral decay is very rapid.

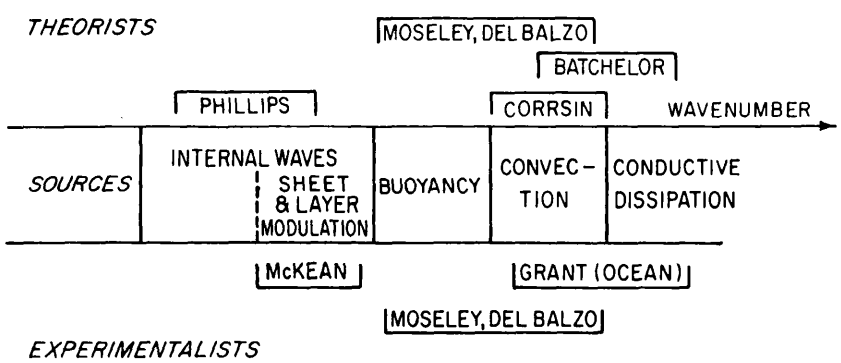


Fig. 10—Major divisions in the spatial spectrum of horizontal temperature fluctuations in a stratified ocean

## CONCLUSIONS

The assumptions, postulates, and dimensional analysis lead to the formulation

$$T_{BC}(k) = BD_\theta \epsilon_0^{-1/3} k^{-5/3} + BCD_\theta N^2 \epsilon_0^{-1} k^{-3}$$

for the horizontal spatial power density spectrum of random oceanic temperature fluctuations in a wavenumber range called the buoyancy-convective range. This range corresponds to the buoyancy-inertial range dealt with in the turbulence theory of stratified fluids.

Analysis of experimental data obtained during 54 horizontal tows with depths ranging from 97.5 to 1454 m at two widely separated stations validates a number of theoretical predictions. Both the -5/3 and -3 predicted power laws were observed; the mean values were -1.68 and -2.94, respectively.

Upon fitting a single-exponent power law formulation over the entire observation range, the expected power law variation between -5/3 and -3 was seen to occur along with the anticipated asymptotic (to -3) nature of the exponent for increasing magnitude of the negative temperature gradient or $N^2$.

The values of the total energy dissipation rate are in good agreement with those which are generally quoted. The new method of calculating $\epsilon_0$, and additionally $D_\theta$, based on least-squares estimates of power law coefficients and the Brunt-Väisälä frequency, appears accurate. A dependence of $\epsilon_0$ and $D_\theta$ on $N$ is also observed, where $\epsilon_0$ ranges from $3.2 \times 10^{-6}$ to $2.0 \times 10^{-4}$ $m^2/s^3$ and $D_\theta$ varies between $4.6 \times 10^{-9}$ and $5.6 \times 10^{-7}$ $°C^2/s$.

The theoretical predictions together with the experimental evidence in this report provide a possible explanation for the disparity in experimental results in the field of random temperature microstructure. A major accomplishment of this work is felt to be that it fills the gap between the wavenumber ranges where internal waves and isotropic turbulence dominate the horizontal spatial random temperature spectrum.

## REFERENCES

1. A. Hecht and R.A. White, "Temperature Fluctuations in the Upper Layer of the Ocean," *Deep-Sea Res.* 15, 339 (1968).

2. S. Neshyba, V.T. Neal, and W.W. Denner, "Spectra of Internal Waves: In-Situ Measurements in a Multiple-Layered Structure," *J. Phys. Ocean.* 2, 91 (1972).

3. R.S. McKean, "Lateral Distributions of Thermal Microstructure in the Open Ocean," APL-UW 7115 (1971).

4. E.C. LaFond and K.G. LaFond, "Thermal Structure Through the California Front, Factors Affecting Underwater Sound Transmission Measured with a Towed Thermistor Chain and Attached Current Meters," NUC TP 224 (1971).

5. C.F. Black, "The Turbulent Distribution of Temperature in the Ocean," Bissett-Berman Corp Report, MJO-1049 (1965).

6. W.B. Moseley and D.R. Del Balzo, "Temperature Microstructure of the Ocean Near the Deep Sound Channel Axis," NRL Report 7729.

7. A.D. Voorhis and H.T. Perkins, "The Spatial Spectrum of Short-wave Temperature Fluctuations in the Near-surface Thermocline," *Deep-Sea Res.* 13, 641 (1966).

8. A.N. Kolmogoroff, "The Local Structure of Turbulence in Incompressible Viscous Fluid for Very Large Reynolds Numbers," *C.R. Acad. Sci. URSS* 30, 301 (1941).

9. G.K. Batchelor, *The Theory of Homogeneous Turbulence*, Cambridge University Press, 1953.

10. J.O. Hinze, "Turbulence: An Introduction to Its Mechanism and Theory," McGraw-Hill, New York, 1959.

11. J.L. Lumley, "The Spectrum of Nearly Inertial Turbulence in a Stably Stratified Fluid," *J. Atmos. Sci.* 21, 99 (1964).

12. O.M. Phillips, *The Dynamics of the Upper Ocean*, Cambridge University Press, 1966.

13. G.N. Shur, "Experimental Investigations of the Energy Spectrum of Atmospheric Turbulence," *TRUDY T.S.: A.O.* 43, 79 (1962).

14. H.L. Grant, R.W. Stewart, and A. Moilliet, "Turbulence Spectra from a Tidal Channel," *J. Fluid Mech.* 12, 241 (1962).

15. H.L. Grant, B.A. Hughes, W.M. Vogel, and A. Moilliet, "The Spectrum of Temperature Fluctuations in Turbulent Flow," *J. Fluid Mech.* 34, 423 (1968).

16. F. Webster, "Turbulence Spectra in the Ocean," *Deep-Sea Res.* 16, 357 (1969).

17. A.M. Obukhov, "The Structure of the Temperature Field in a Turbulent Stream," Izv. Akad. Nauk. SSSR, *Geogr. i Geofiz.* 13, 58 (1949).

18. S. Corrsin, "On the Spectrum of Isotropic Temperature Fluctuations in an Isotropic Turbulence," *J. Applied Physics* 22, 469 (1951).

19. G.K. Batchelor, "Small-scale Variations of Convected Quantities Like Temperature in Turbulent Fluid," *J. Fluid Mech.* 5, 113 (1959).

20. C.H. Gibson and W.H. Schwarz, "The Universal Equilibrium Spectra of Turbulent Velocity and Scalar Fields," *J. Fluid Mech.* 16, 365 (1963).

21. O.M. Phillips, "On Spectra Measured in an Undulating Layered Medium," *J. Phys. Ocean.* 1, 1 (1971).

22. C. Garrett and W. Munk, "Internal Wave Spectra in the Presence of Fine-Structure," *J. Phys. Ocean.* 1, 196 (1971).

## Appendix A
## INSTRUMENTATION, EXPERIMENTAL TECHNIQUES, AND DATA REDUCTION

In the fall of 1970, the USNS *Mizar* was deployed in the Bermuda Rise area of the North Atlantic for the purpose of gathering data on random environmental fluctuations. From October 29 until November 12, measurements were taken in the rectangle extending from 31° 45′N to 32° 15′N and from 63° 55′W to 64° 35′W (Station 1). During November 13-19, the operating area was between 29° 05′N, 29° 35′N, 66° 35′W, and 67° 15′W (Station 2).

The *Mizar* is particularly well suited for this kind of experiment due to its center-well towing capability. With the tow point located near the ship's center of gravity, the rotational components of ship motion are partially decoupled from the instrument package. Frequently, with the *Mizar* drifting, the instruments were raised or lowered over large depth intervals in order to obtain vertical profiles. This was done at many locations and the results showed no significant changes between profiles at various points within a station. The average profiles for each station are given in Fig. A1.

At each station a series of straight-line tow runs was executed over a wide range of depths, speeds, and distances. The important characteristics of each run are presented in Table A1. Excessive cable fatigue due to strumming was encountered during the 4-knot runs, and consequently an upper limit of 3 knots was set for the remainder of the tows. Before and after each run, the instruments were raised and lowered several times around the tow depth in order to obtain a "local" (run by run) record of the vertical temperature gradient and, with archival salinity data, the Brunt-Väisälä frequency. These results are shown in Fig. A2, where each point represents an average over many runs at a similar depth.

The instruments were attached to the front of a streamlined fish which was designed and constructed at NRL. The weight of the tow body is adjusted for each operational depth, since good towing stability requires more weight for the deep depths than for the shallow depths. Throughout each tow run the pressure sensor output is monitored and minor cable length adjustments are made to insure a relatively constant tow depth. Figure A3 shows the tow body and four sensors.

The three environmental sensors are a platinum resistance temperature probe, a velocimeter, and a vibrotron pressure transducer. Calibrations were conducted at NRL both before and after the experiment and no statistically significant changes were measured.* The fourth sensor is a Savonius rotor current meter which is used to measure the rate of motion through the fluid.

---

*For more details on the environmental sampling technique and explanations of the calibration and data gathering procedures, see Moseley and Del Balzo (A2).

Table A1
Run Statistics, 1970

| Run | Average Depth (m) | Average Speed (knots) | Duration (Hrs.) | Distance Sampled (n.mi.) | Speed Quality (%) | Depth Quality (%) | Equivalent Number of Degrees of Freedom | Noise Level ($\times 10^6$) ($^\circ C^2$-m.) | Number of Data Points in Average |
|---|---|---|---|---|---|---|---|---|---|
| 1-150-1 | 142 | 4.7 | 2.4 | 11.2 | 3 | 5.6 | 39 | 3.3 | 40960 |
| 1-150-2 | 145 | 4.7 | 3.4 | 16.0 | 8 | 10.3 | 57 | 3.2 | 61440 |
| 1-150-3 | 142 | 4.6 | 3.4 | 15.4 | 3 | 4.2 | 51 | 3.5 | 53242 |
| 1-300-1 | 290 | 4.6 | 3.2 | 14.7 | 5 | 25.2 | 39 | 5.1 | 40960 |
| 1-300-2 | 286 | 4.8 | 3.4 | 16.4 | 3 | 7.7 | 57 | 5.6 | 61440 |
| 1-300-3 | 315 | 4.2 | 3.2 | 13.6 | 5 | 12.4 | 49 | 2.1 | 53248 |
| 1-300-4 | 310 | 4.4 | 3.0 | 13.3 | 3 | 5.8 | 49 | 4.8 | 53248 |
| 1-400-1 | 387 | 4.1 | 3.3 | 13.5 | 3 | 5.2 | 55 | 1.9 | 57344 |
| 1-400-2 | 355 | 4.6 | 6.3 | 28.8 | 5 | 10.7 | 104 | 2.4 | 110592 |
| 1-400-3 | 382 | 4.2 | 3.8 | 15.8 | 3 | 17.0 | 39 | 3.0 | 40960 |
| 1-400-4 | 390 | 2.3 | 5.3 | 12.2 | 5 | 3.6 | 63 | 1.3 | 65536 |
| 1-550-2 | 626 | 2.1 | 3.5 | 7.3 | 3 | 7.5 | 51 | 2.7 | 53248 |
| 1-550-3 | 650 | 2.1 | 4.6 | 9.6 | 3 | 13.1 | 61 | 2.5 | 65536 |
| 1-550-4 | 551 | 1.8 | 5.2 | 9.3 | 3 | 2.6 | 79 | 1.9 | 81920 |
| 1-750-1 | 721 | 3.1 | 3.0 | 9.2 | 3 | 2.9 | 49 | 3.2 | 53248 |
| 1-750-2 | 718 | 2.4 | 5.6 | 13.4 | 5 | 7.7 | 63 | 4.8 | 65536 |
| 1-750-3 | 730 | 2.3 | 5.5 | 12.7 | 5 | 4.1 | 65 | 4.8 | 69632 |
| 1-750-4 | 727 | 2.4 | 5.2 | 12.4 | 3 | 1.0 | 79 | 3.2 | 81920 |
| 1-900-1 | 870 | 2.4 | 2.6 | 6.3 | 3 | 3.7 | 35 | 3.5 | 36864 |
| 1-900-2 | 872 | 2.3 | 5.5 | 12.7 | 3 | 2.8 | 87 | 1.9 | 90112 |
| 1-900-3 | 875 | 2.6 | 4.9 | 12.9 | 3 | 1.4 | 81 | 3.2 | 86016 |
| 1-900-4 | 875 | 2.7 | 2.8 | 7.7 | 3 | 1.0 | 43 | 2.5 | 45056 |
| 1-900-5 | 872 | 2.3 | 5.7 | 13.1 | 3 | 1.3 | 96 | 2.1 | 102400 |
| 1-1100-1 | 1067 | 1.9 | 2.3 | 4.3 | 3 | 1.9 | 28 | 1.9 | 28672 |
| 1-1100-2 | 1067 | 2.5 | 1.6 | 4.0 | 3 | 1.9 | 26 | 1.6 | 28672 |
| 1-1100-4 | 1067 | 2.2 | 2.7 | 5.9 | 3 | 1.4 | 43 | 2.1 | 45056 |
| 1-1100-5 | 1071 | 2.8 | 1.3 | 3.7 | 3 | 1.9 | 22 | 4.1 | 24576 |
| 1-1100-6 | 1072 | 3.0 | 1.6 | 4.8 | 3 | 1.4 | 26 | 2.4 | 28672 |
| 1-1100-7 | 1066 | 3.0 | 2.2 | 6.5 | 3 | 1.5 | 35 | 1.9 | 36864 |
| 1-1300-1 | 1266 | 2.6 | 6.1 | 15.8 | 3 | 1.3 | 94 | 2.4 | 98304 |
| 1-1300-2 | 1260 | 2.6 | 4.8 | 12.4 | 3 | 1.0 | 81 | 2.4 | 86016 |
| 1-1300-3 | 1264 | 2.9 | 4.8 | 13.9 | 3 | 1.4 | 81 | 2.4 | 86016 |
| 1-1500-1 | 1453 | 1.7 | 4.1 | 17.0 | 5 | 0.7 | 69 | 2.2 | 73728 |
| 1-1500-2 | 1454 | 2.7 | 3.3 | 8.9 | 3 | 0.6 | 55 | 2.1 | 57344 |
| 1-1500-3 | 1452 | 1.8 | 2.3 | 4.1 | 5 | 0.2 | 33 | 1.4 | 36864 |
| 1-1500-4 | 1453 | 2.2 | 3.4 | 7.4 | 5 | 0.7 | 53 | 1.9 | 57344 |
| 1-1500-5 | 1453 | 2.1 | 3.3 | 6.9 | 3 | 0.2 | 53 | 1.3 | 57344 |
| 2-100-1 | 98.3 | 2.3 | 2.3 | 5.2 | 3 | 0.5 | 37 | 2.1 | 40960 |
| 2-100-2 | 97.6 | 2.3 | 6.0 | 13.9 | 3 | 0.4 | 96 | 2.1 | 102400 |
| 2-100-3 | 97.5 | 2.2 | 6.3 | 13.9 | 5 | 0.5 | 102 | 2.2 | 106496 |
| 2-100-4 | 98.4 | 2.0 | 4.0 | 8.0 | 3 | 1.0 | 59 | 1.8 | 61440 |
| 2-300-1 | 292 | 1.8 | 7.1 | 12.7 | 3 | 1.4 | 106 | 2.1 | 110592 |
| 2-300-2 | 292 | 2.5 | 3.8 | 9.5 | 3 | 1.0 | 57 | 2.1 | 61440 |
| 2-600-1 | 583 | 2.5 | 5.5 | 13.7 | 3 | 0.9 | 92 | 1.9 | 98304 |
| 2-600-2 | 583 | 1.9 | 6.3 | 11.9 | 3 | 1.2 | 106 | 1.9 | 110592 |
| 2-600-3 | 584 | 2.0 | 7.1 | 14.2 | 3 | 0.9 | 110 | 2.2 | 114688 |
| 2-900-1 | 875 | 2.7 | 4.9 | 13.4 | 3 | 0.7 | 83 | 1.8 | 86016 |
| 2-900-2 | 875 | 2.3 | 5.7 | 13.1 | 3 | 0.8 | 96 | 2.4 | 102400 |
| 2-1200-1 | 1165 | 2.1 | 5.1 | 10.8 | 3 | 0.8 | 87 | 1.9 | 90112 |
| 2-1200-2 | 1164 | 2.4 | 3.2 | 7.6 | 3 | 0.4 | 53 | 2.4 | 57344 |
| 2-1200-3 | 1164 | 2.5 | 5.2 | 13.0 | 3 | 0.9 | 83 | 2.1 | 86016 |
| 2-1200-4 | 1165 | 2.7 | 2.4 | 6.5 | 3 | 0.3 | 39 | 1.4 | 40960 |
| 2-1500-1 | 1454 | 2.2 | 5.2 | 11.5 | 3 | 0.6 | 89 | 0.8 | 94208 |
| 2-1500-2 | 1454 | 2.1 | 5.8 | 12.2 | 3 | 0.7 | 94 | 0.6 | 102400 |

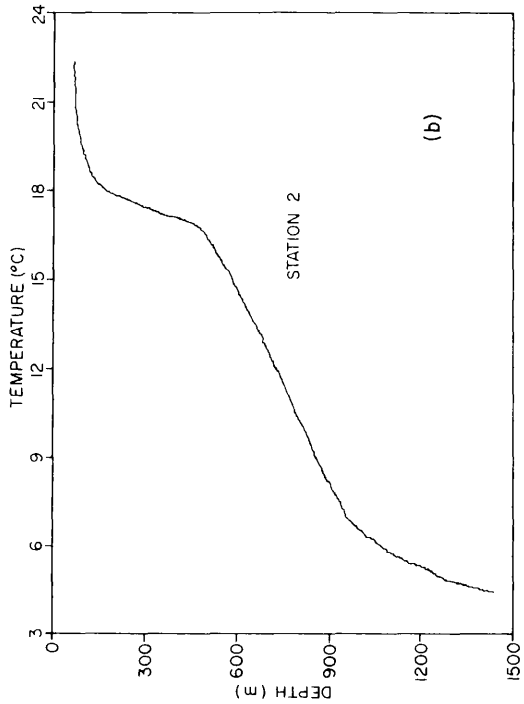
TEMPERATURE (°C)
3
6
9
12
15
18
21
24
STATION 2
(b)
DEPTH (m)
0
300
600
900
1200
1500

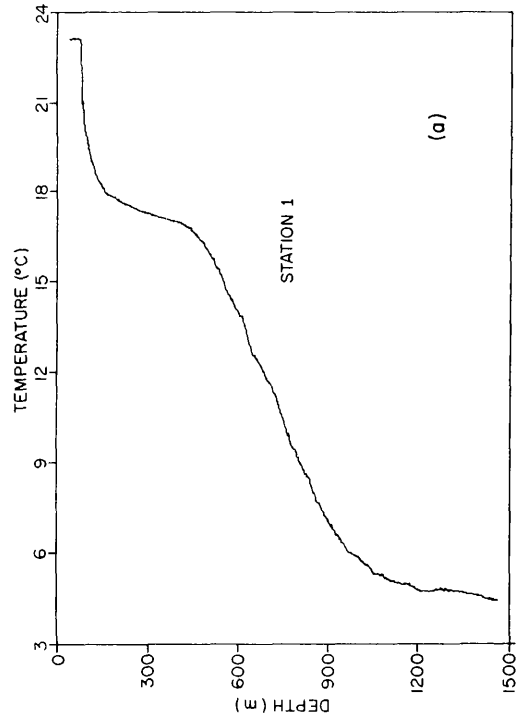
TEMPERATURE (°C)
3
6
9
12
15
18
21
24
STATION 1
(a)
DEPTH (m)
0
300
600
900
1200
1500

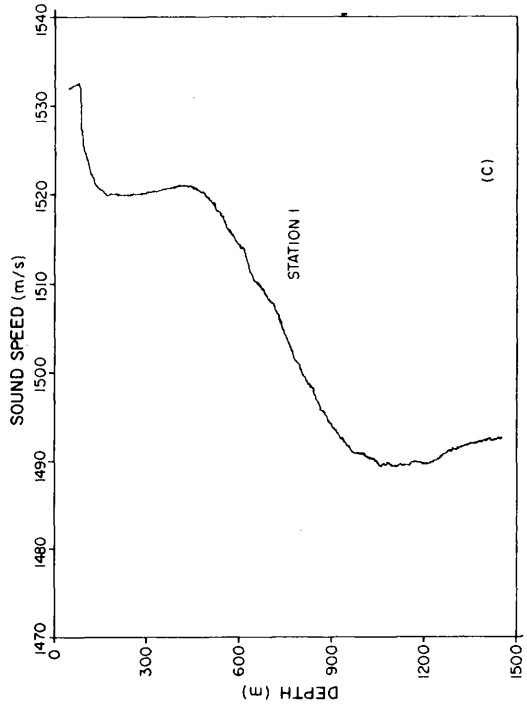
SOUND SPEED (m/s)
1470
1480
1490
1500
1510
1520
1530
1540
STATION 1
(c)
DEPTH (m)
0
300
600
900
1200
1500

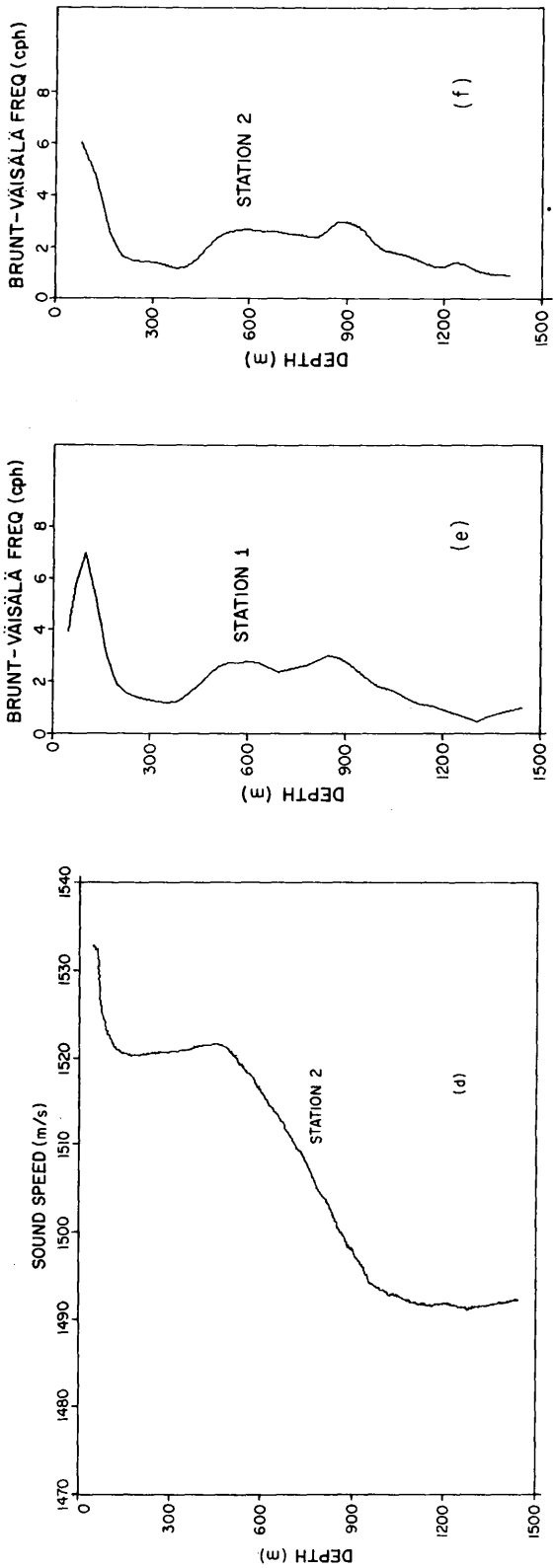


Fig. A1 — Mean profiles during the experiment: (a) temperature at Station 1; (b) temperature at Station 2; (c) sound speed at Station 1; (d) sound speed at Station 2; (e) Brunt-Väisälä frequency at Station 1; (f) Brunt Väisälä frequency at Station 2

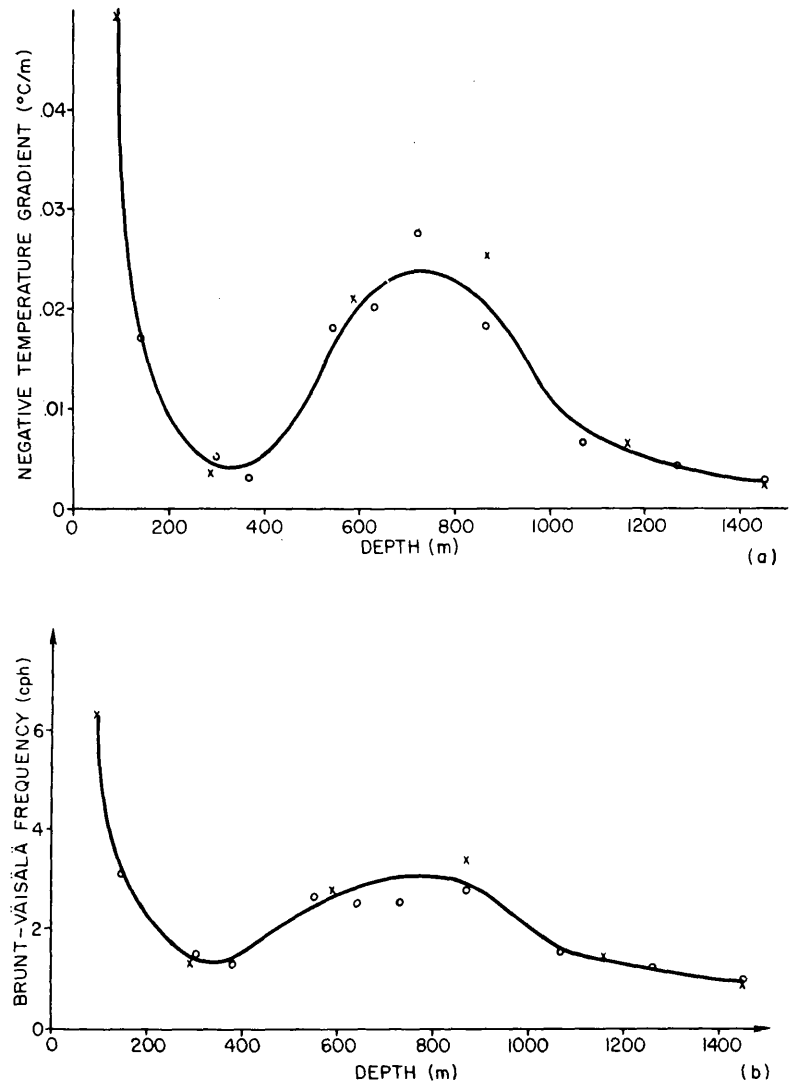


Fig. A2—Run-by-run profiles of (a) negative temperature gradient, and (b) Brunt-Väisälä frequency (0 = Station 1, $x$ = Station 2)

The environmental sensors sample the medium five times a second and return FM signals through a coaxial cable for shipboard processing and digital recording. The on-line displays of data are Nixie tubes, Brush recorders, and oscilloscope traces. The analog current meter output is recorded on a Brush recorder.

The data reduction process begins, through the use of the calibration equations, with the conversion of the digital raw data into pressure in pounds per square inch, sound speed in meters per second, and temperature in degrees Centigrade. Each pressure sample is also converted into a depth in meters. Utilizing local temperature-salinity diagrams, each corresponding value of temperature and depth is used in Wilson's equation (A1) to calculate

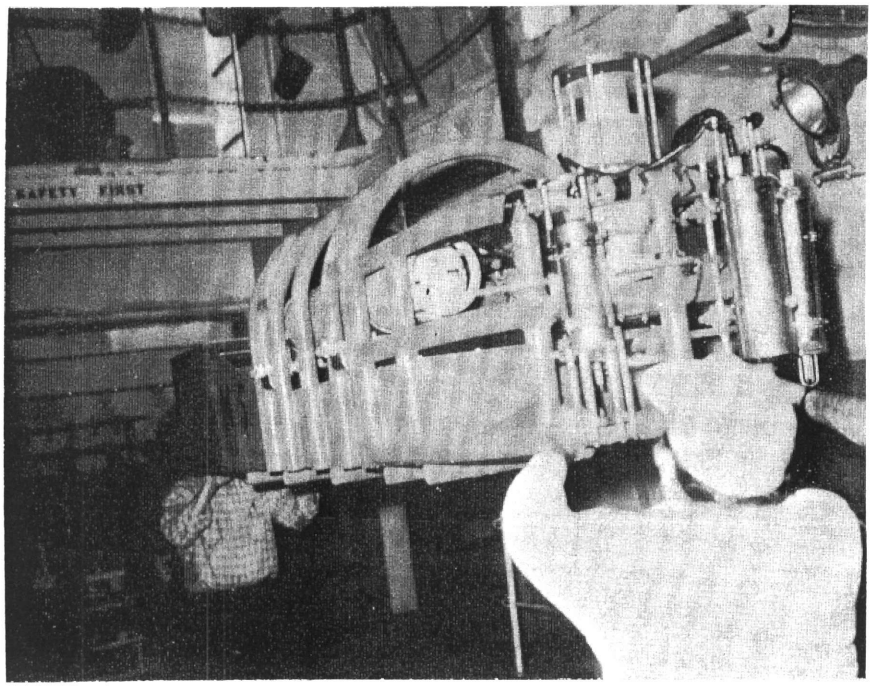


Fig. A3—Tow body showing three environmental sensors, current meter, and battery pack

a sound speed which is compared to the measured sound speed. This provides a continuing check on the functioning of all three sensors. The average depth and temperature during each record (1024 data samples) is plotted against the record number so that any trends or discontinuities will be apparent (see Fig. A4). The current-meter signal is converted into a speed, averaged over each record, and plotted vs record number as in Fig. A5 (upper trace). The lower points represent consecutive overlapped segment averages (a segment equals four records). Unusual speed and/or depth discontinuities or trends are cause for removal of data segments from further analysis.

The analysis* involves power spectral density computations as a function of spatial wavenumber $k$. The power spectra are obtained by the direct method of power spectral computation (A3) which utilizes the fast Fourier transform. A segment (4096 data points = 13.7 min) is used as the basic time series for each transform. An analysis window (A2) with extremely low side-lobe structure (first side lobe at -58.1 dB re main lobe) is applied in a direct manner to 50% overlapped segments during the transform process after removal of a mean and linear trend. The nearly independent transforms are then converted into power spectral density estimates and averaged to give $\hat{T}_{BC}(k)$ (caret indicates raw estimate).

The raw estimates of the temperature power spectral density, $\hat{T}_{BC}(k)$ are, to varying degrees, contaminated by pseudotemperature fluctuations caused by depth variations in

*A detailed treatment of the analysis technique is given in Ref. A2.

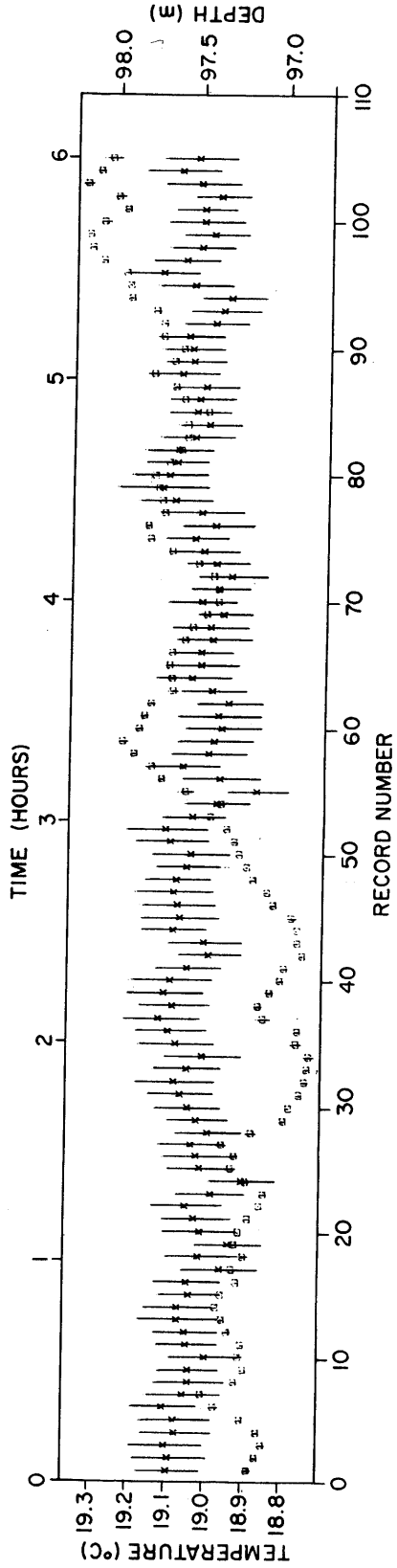


Fig. A4—Average depth ($X$) and temperature (□) during each record with $1\sigma$ error bars

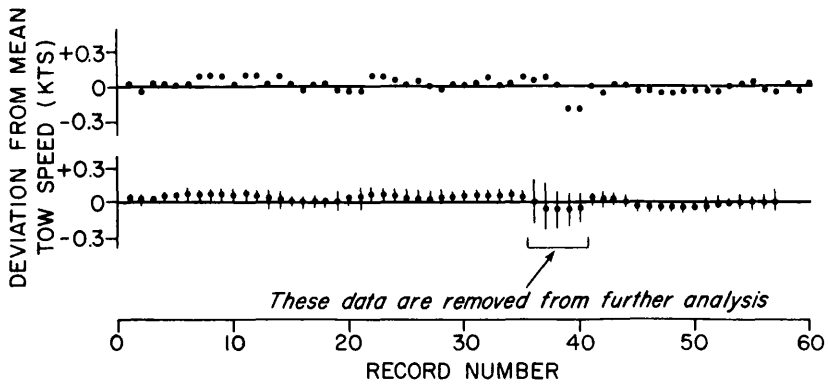


Fig. A5—Deviation from mean tow speed of run averaged over one record (top trace) and averaged over consecutive overlapped 4-record segments with error bars (bottom trace).

the presence of a complicated vertical temperature structure. A measure of the contamination is obtained through cross-spectral analysis between temperature and depth. In particular, the squared coherency spectrum $K^2_{TD}$,* which is a nondimensional measure of the linear correction between the two spectra,† is used to obtain a better estimate of $T_{BC}(k)$, the true random temperature power density spectrum, given by

$$T_{BC}(k) = \hat{T}_{BC}(k)[1 - K^2_{TD}(k)].$$

The results of the analysis applied to the tow run are shown graphically in Appendix B.

## REFERENCES

A1. W.D. Wilson, "Speed of Sound in Sea Water as a Function of Temperature, Pressure, and Salinity," JASA 32, 641 (1960).

A2. W.B. Moseley and D.R. Del Balzo, "Temperature Microstructure of the Ocean Near the Deep Sound Channel Axis," NRL Report 7729.

A3. W.B. Moseley, "Direct Computation of Power Density and Energy Density Spectra," NRL Report 7179, Mar. 1971.

*$K^2_{TD}(k) = [\mathrm{Co}^2(k) + \mathrm{Quad}^2(k)]/\hat{T}_{BC}(k)D_{BC}(k)$, where $\mathrm{Co}(k)$ is the cospectrum, $\mathrm{Quad}(k)$ is the quadrature spectrum, $\hat{T}_{BC}(k)$ is the previously defined raw temperature power density, and $D_{BC}(k)$ is the depth power density spectrum in the buoyancy-convective range.

†$K^2_{TD}$ is restricted to the interval [0,1], wherein

$$K^2_{TD} = \begin{cases} 0 \text{ implies spectra completely uncorrelated} \\ 1 \text{ implies spectra fully correlated.} \end{cases}$$

## Appendix B
## TEMPERATURE POWER SPECTRAL DENSITY PLOTS

Contained herein are spatial power spectral density plots of temperature fluctuations with 95% confidence limits. For ease in converting to distance (size scale) the power is presented with units ($^{\circ}C^2$/cpm) and wavenumber is given with units (cpm). The run identification is presented in the upper right-hand corner of each plot.

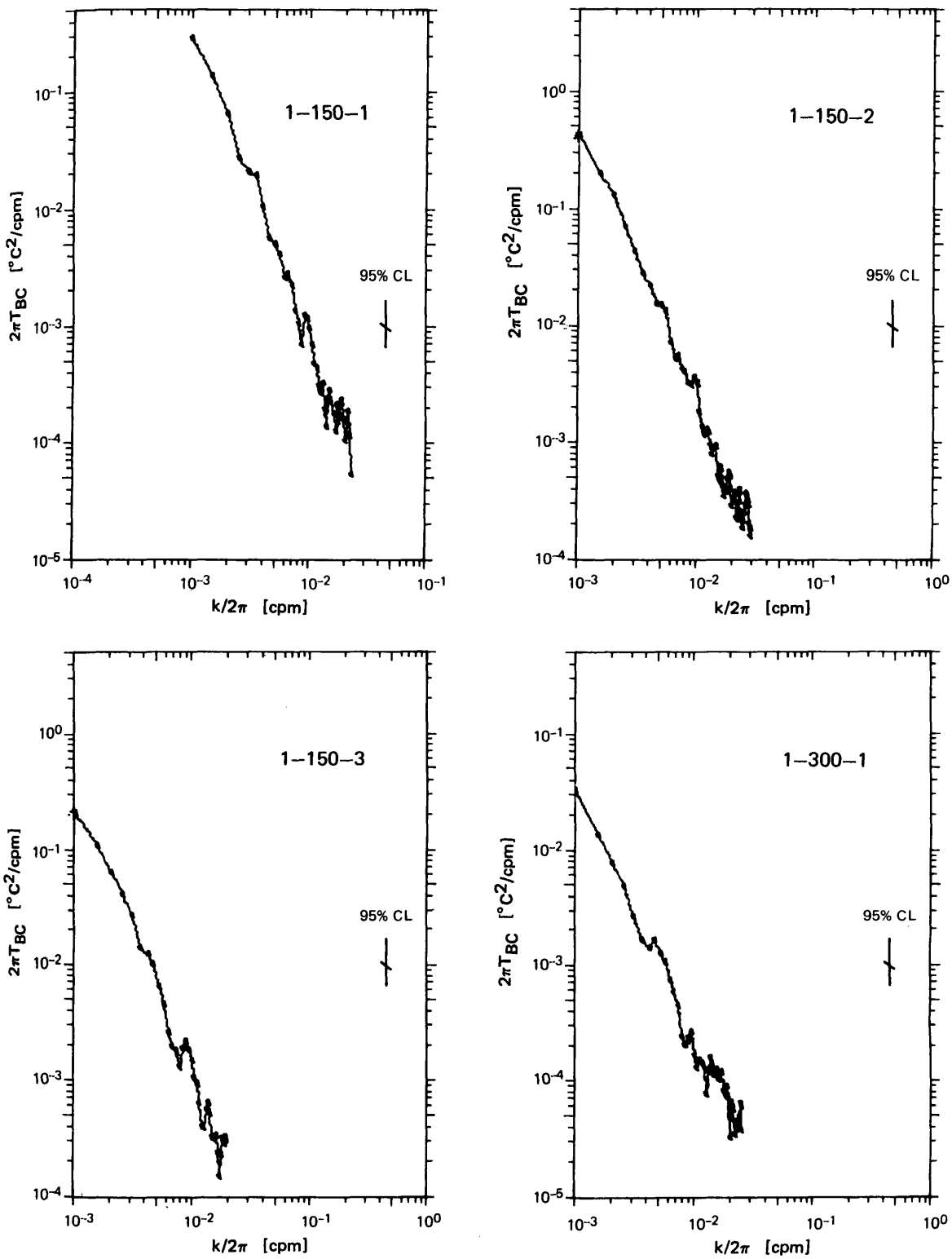


Fig. B1—Temperature power spectral density plots with 95% confidence limits.

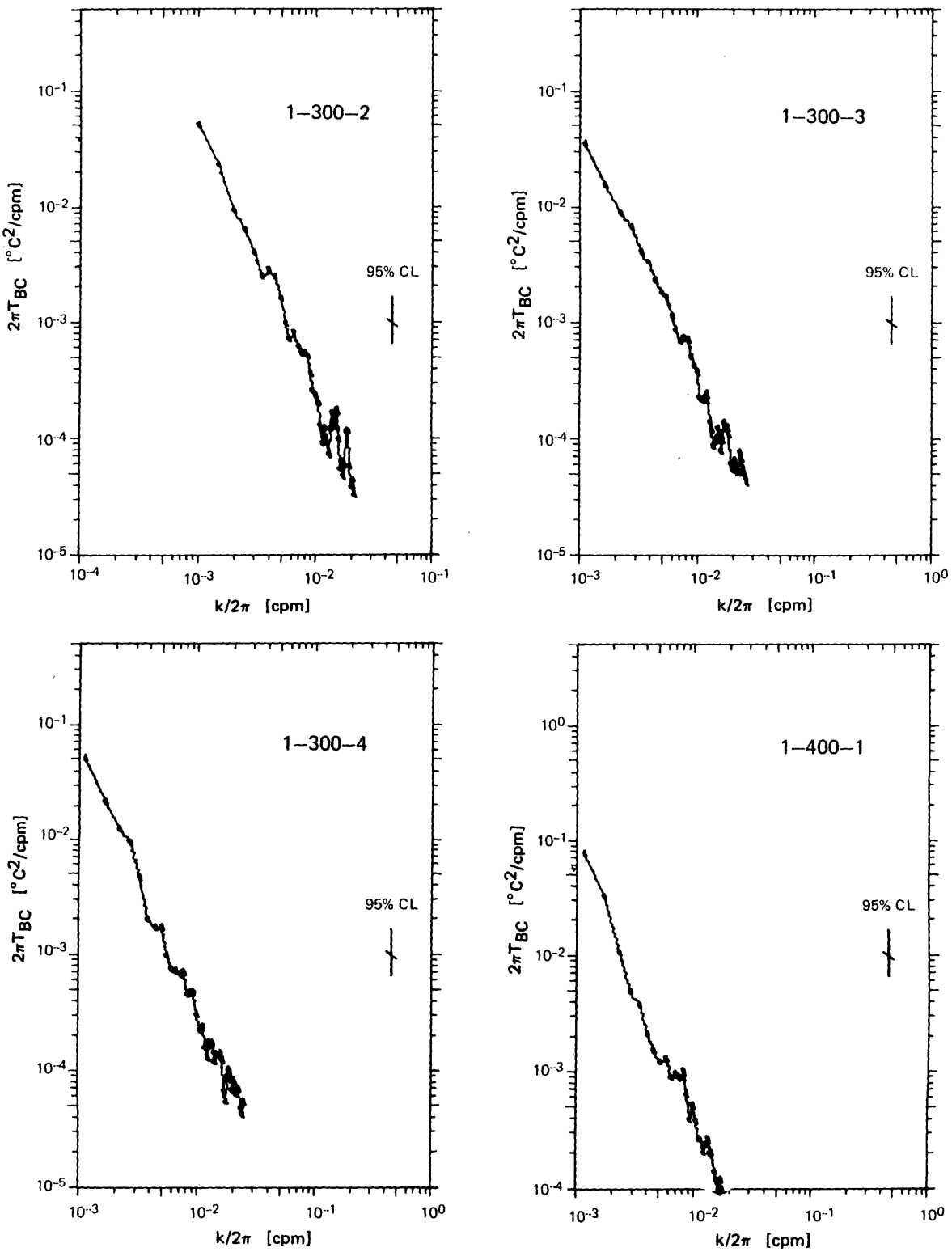


Fig. B1—Temperature power spectral density plots with 95% confidence limits (Continued).

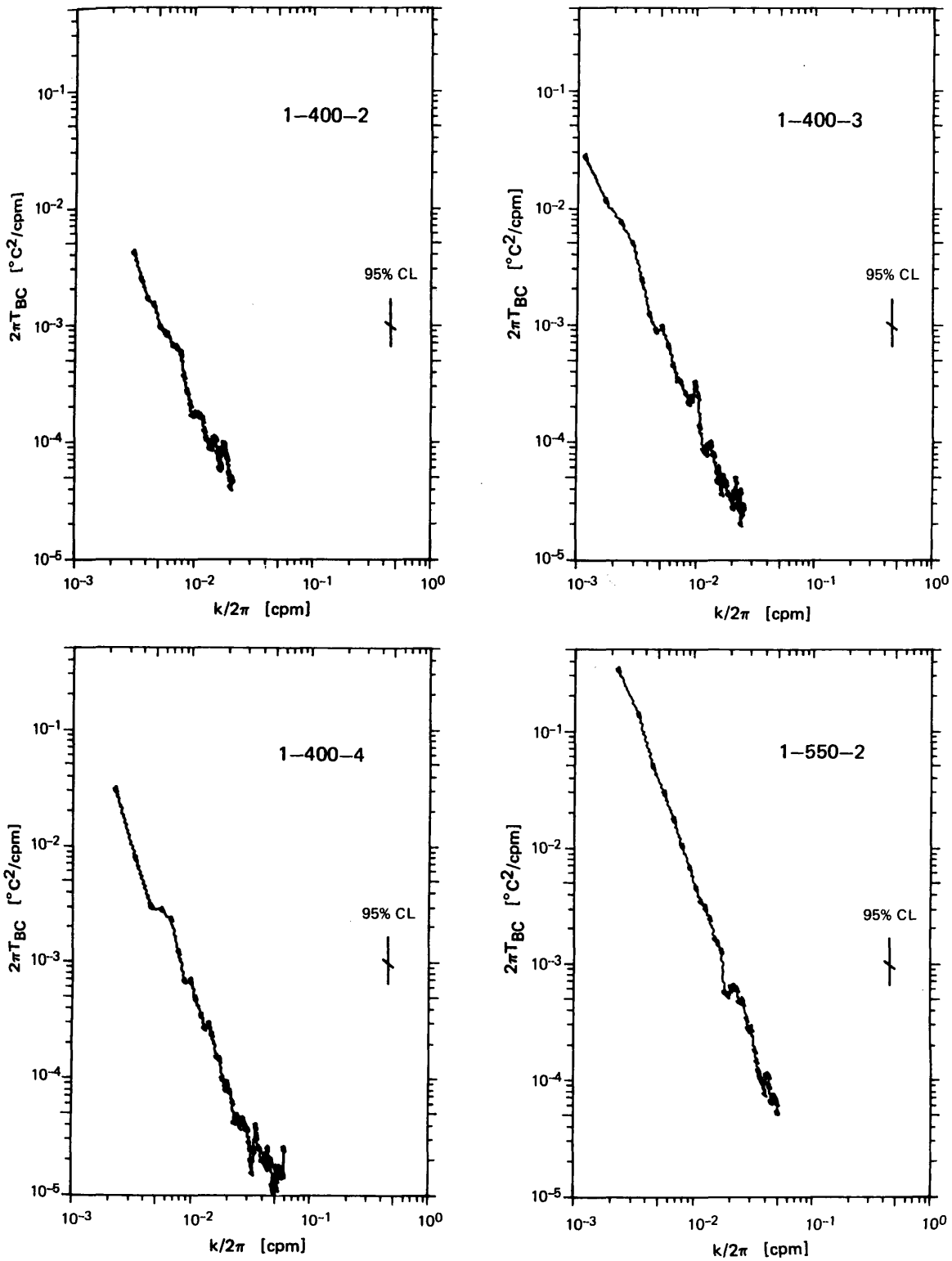


Fig. B1—Temperature power spectral density plots with 95% confidence limits (Continued)

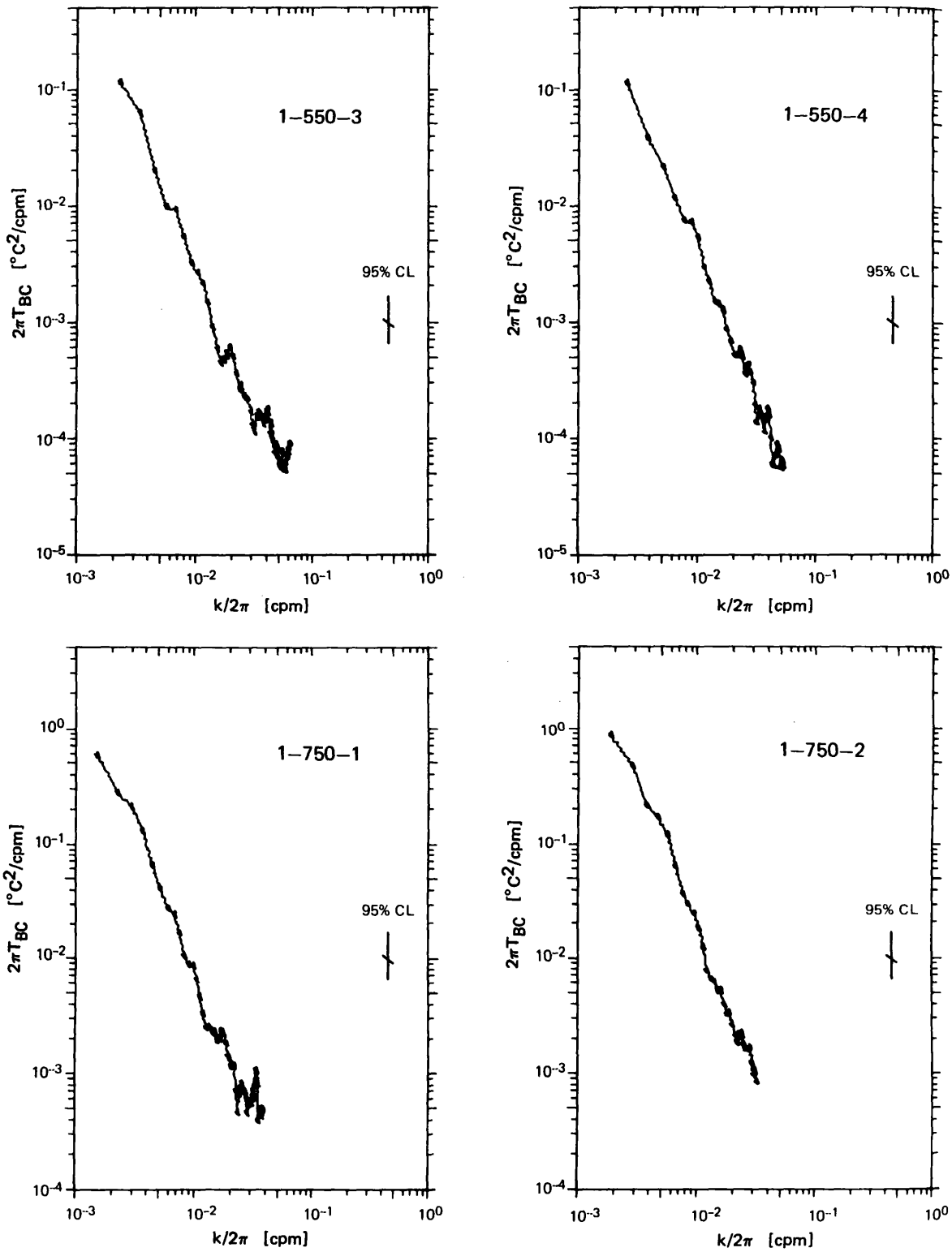


Fig. B1—Temperature power spectral density plots with 95% confidence limits (Continued).

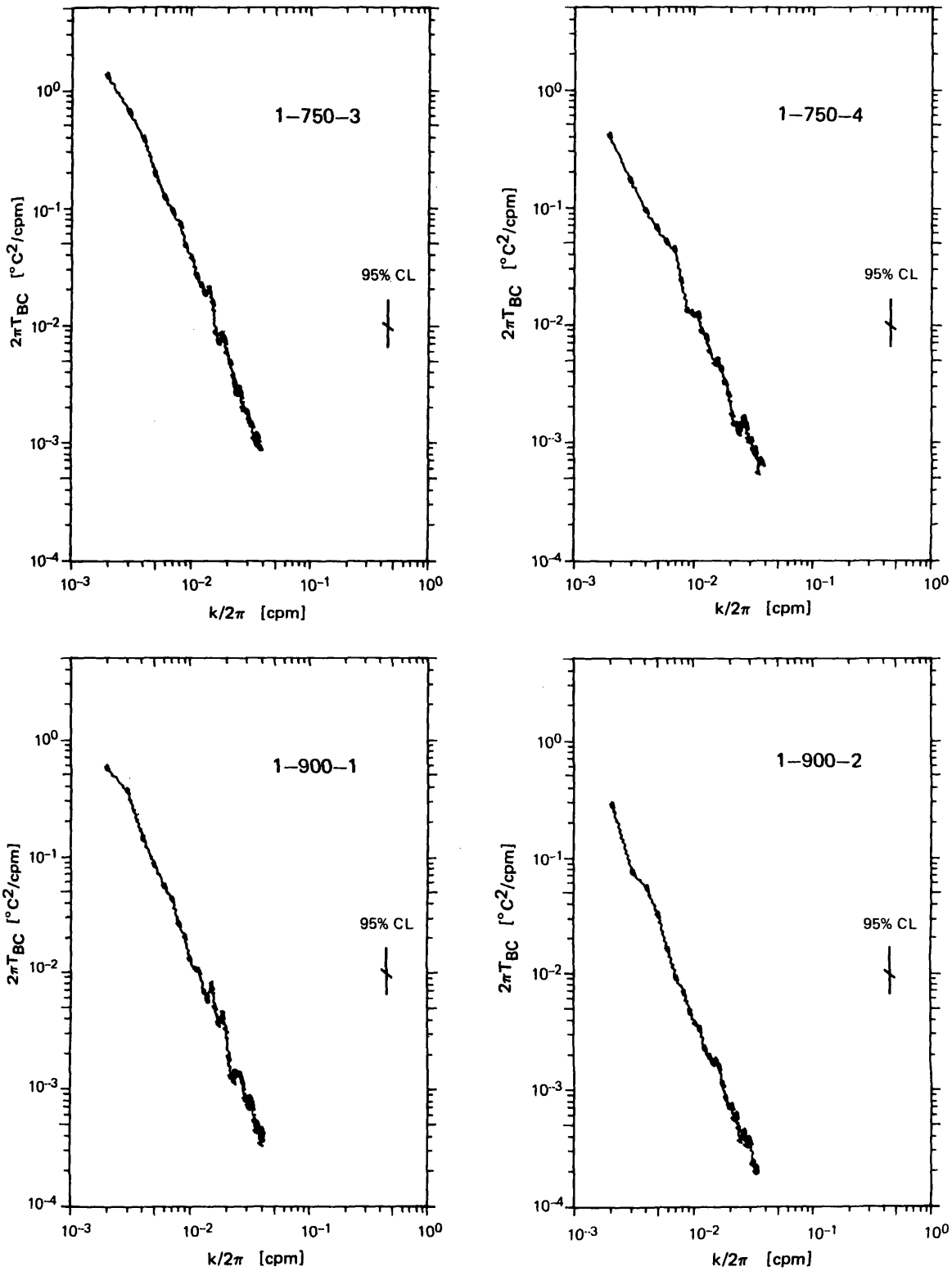


Fig. B1—Temperature power spectral density plots with 95% confidence limits (Continued).

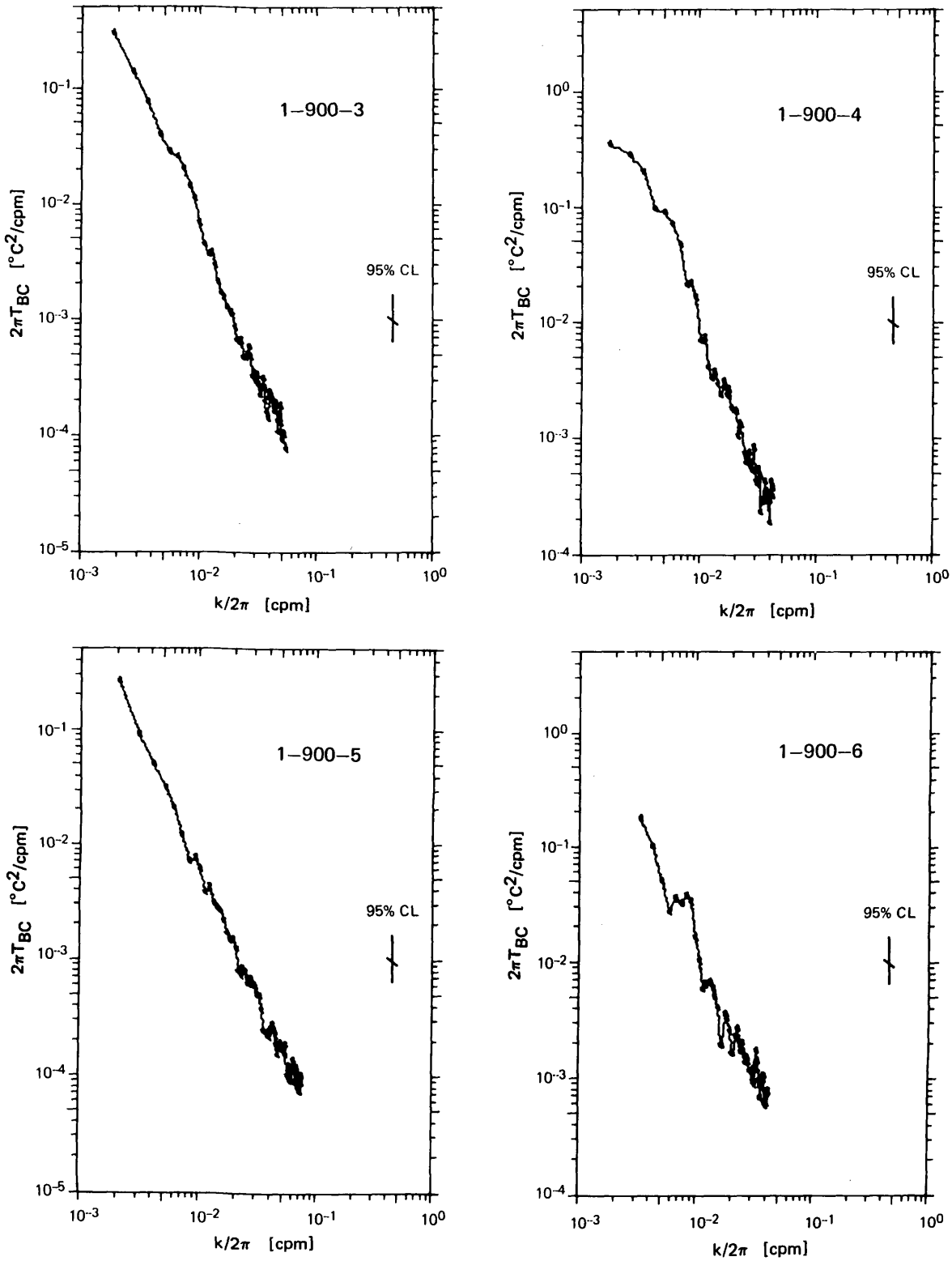


Fig. B1—Temperature power spectral density plots with 95% confidence limits (Continued).

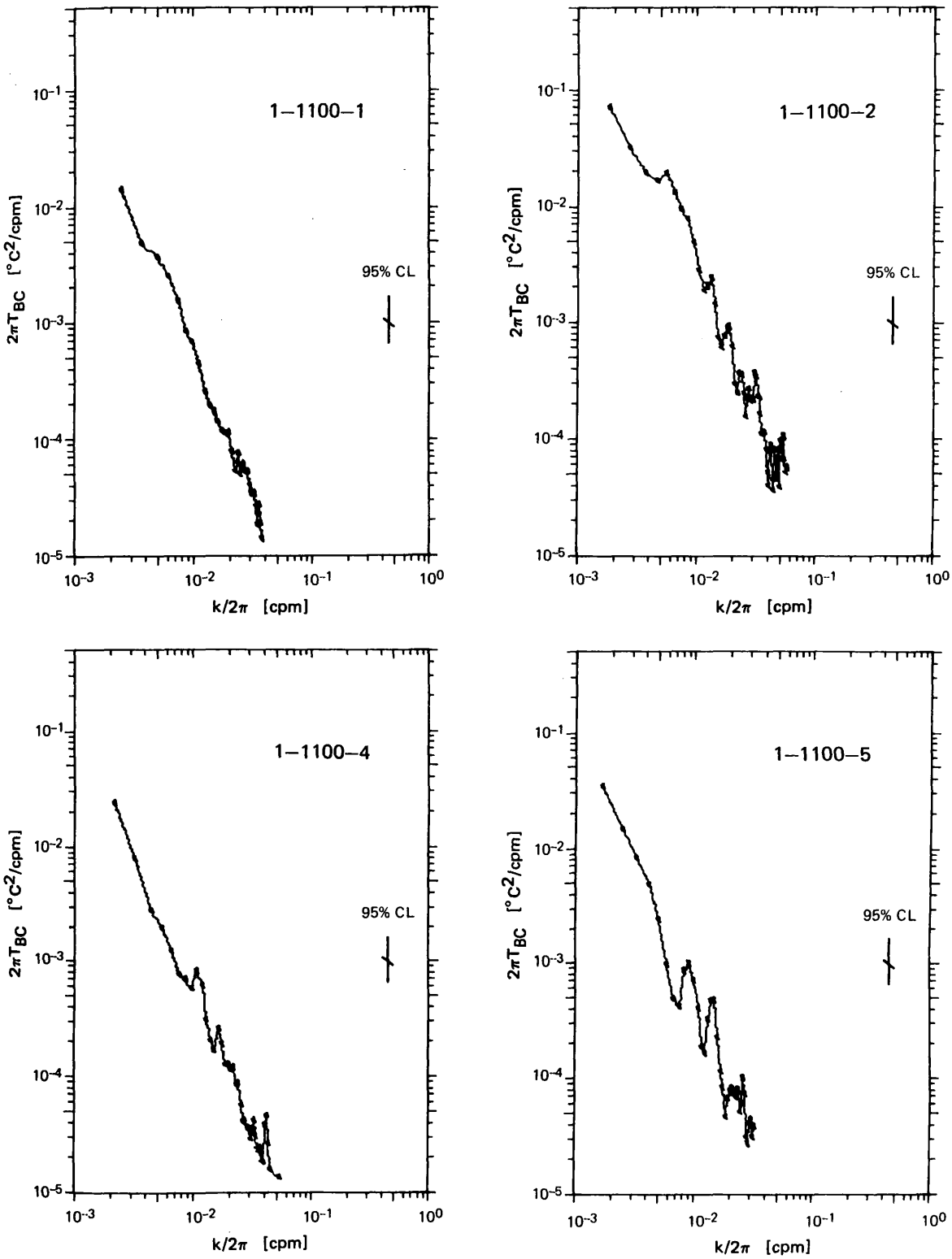


Fig. B1—Temperature power spectral density plots with 95% confidence limits (Continued)

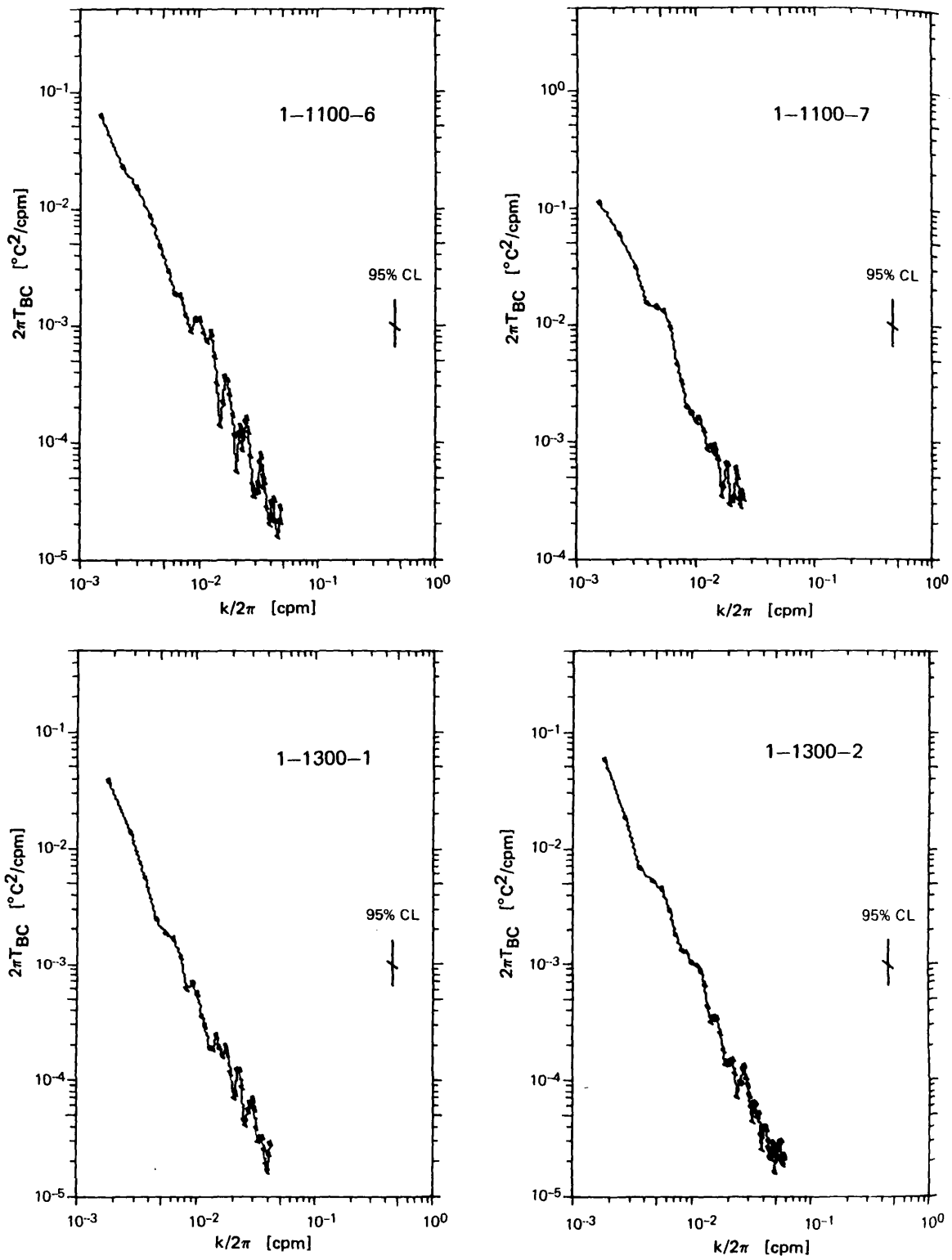


Fig. B1—Temperature power spectral density plots with 95% confidence limits (Continued)

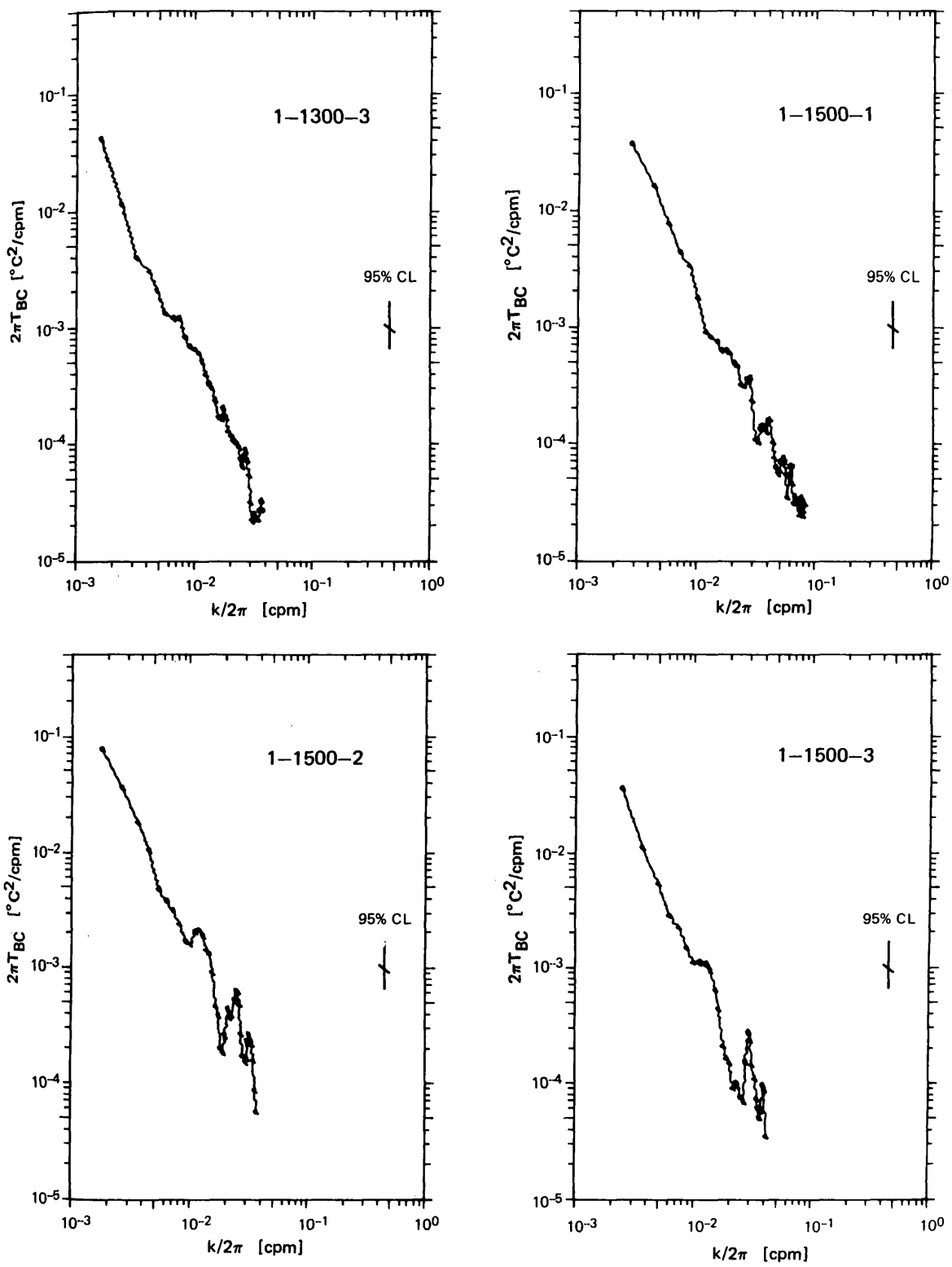


Fig. B1—Temperature power spectral density plots with 95% confidence limits (Continued)

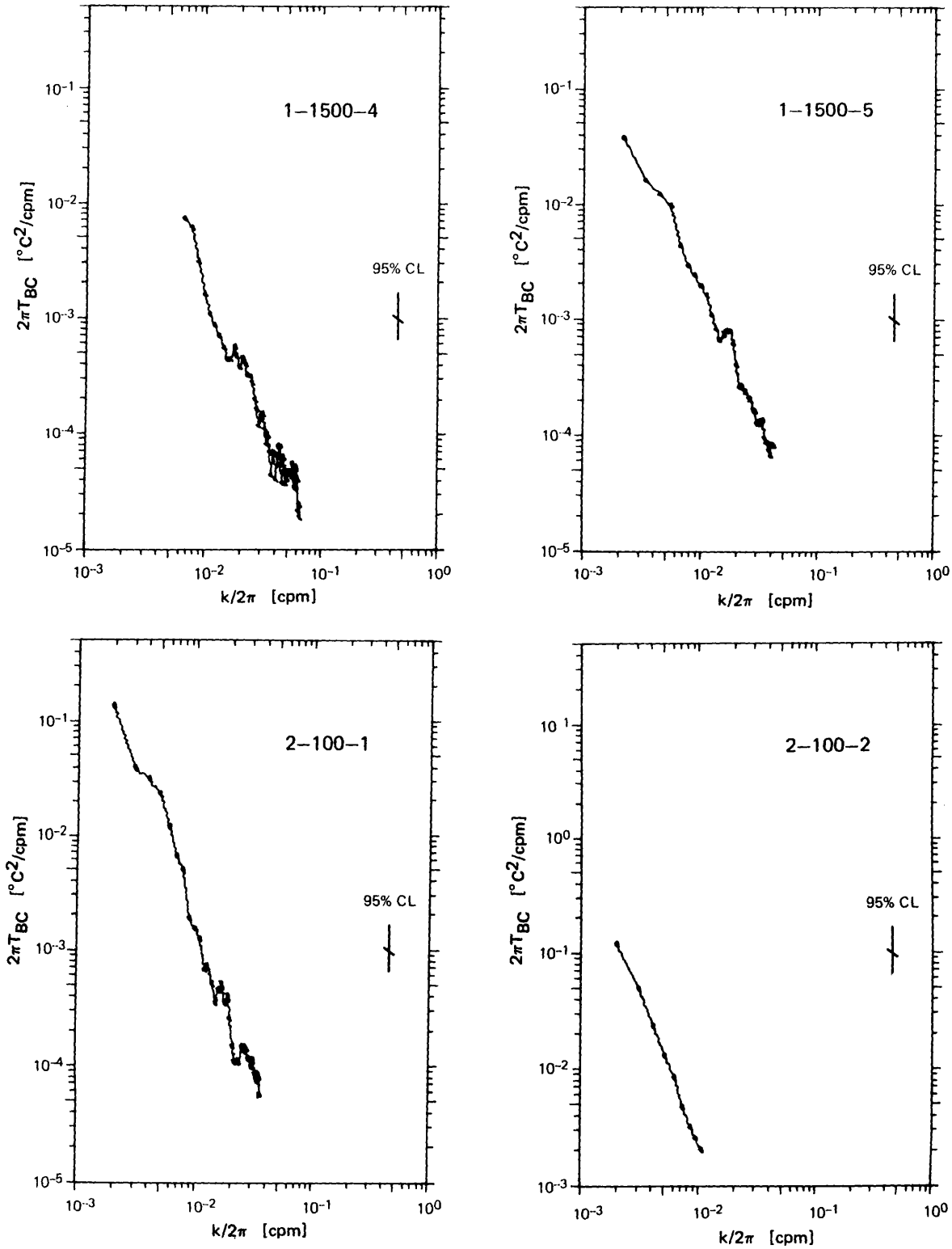


Fig. B1—Temperature power spectral density plots with 95% confidence limits (Continued)

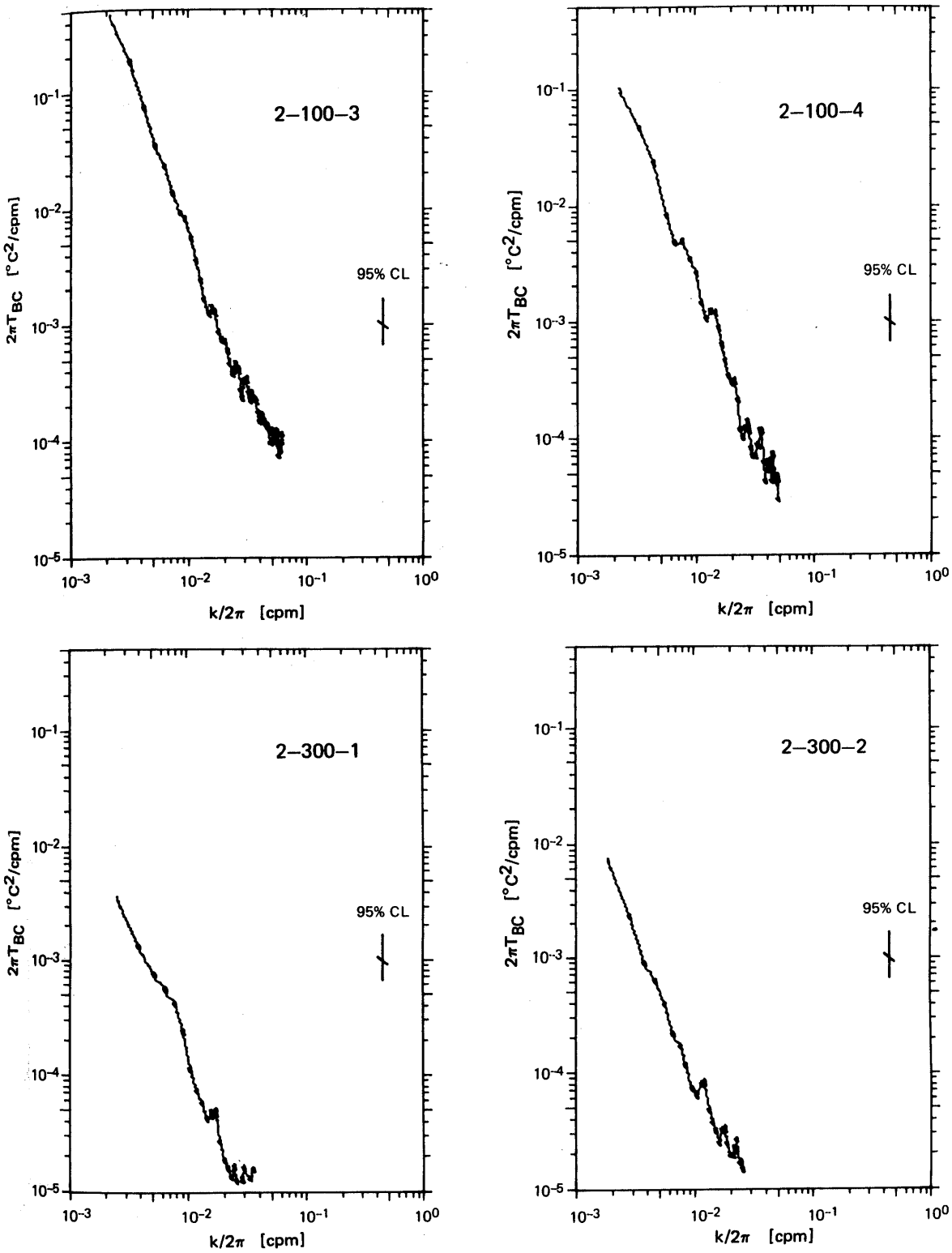


Fig. B1—Temperature power spectral density plots with 95% confidence limits (Continued)

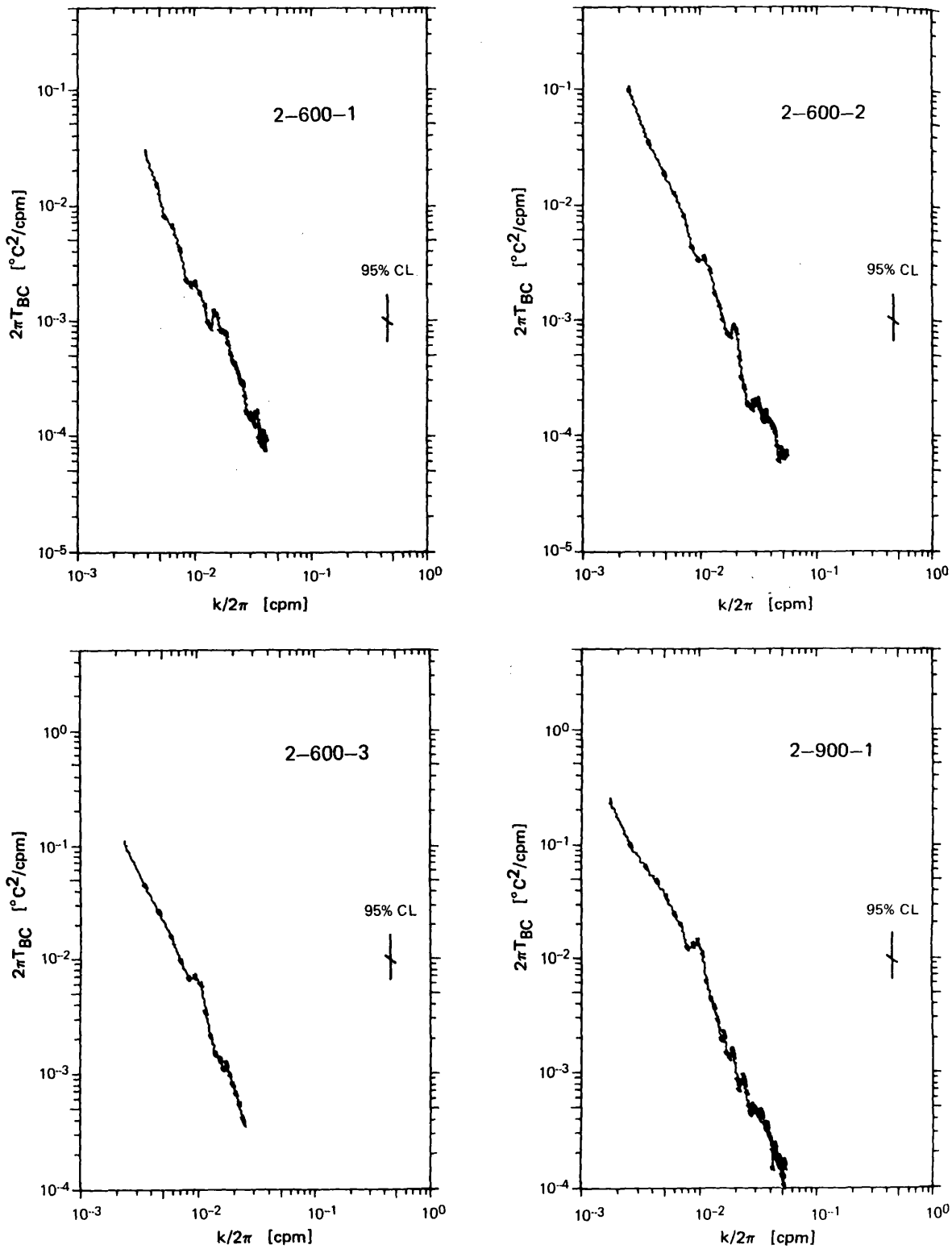


Fig. B1—Temperature power spectral density plots with 95% confidence limits (Continued)

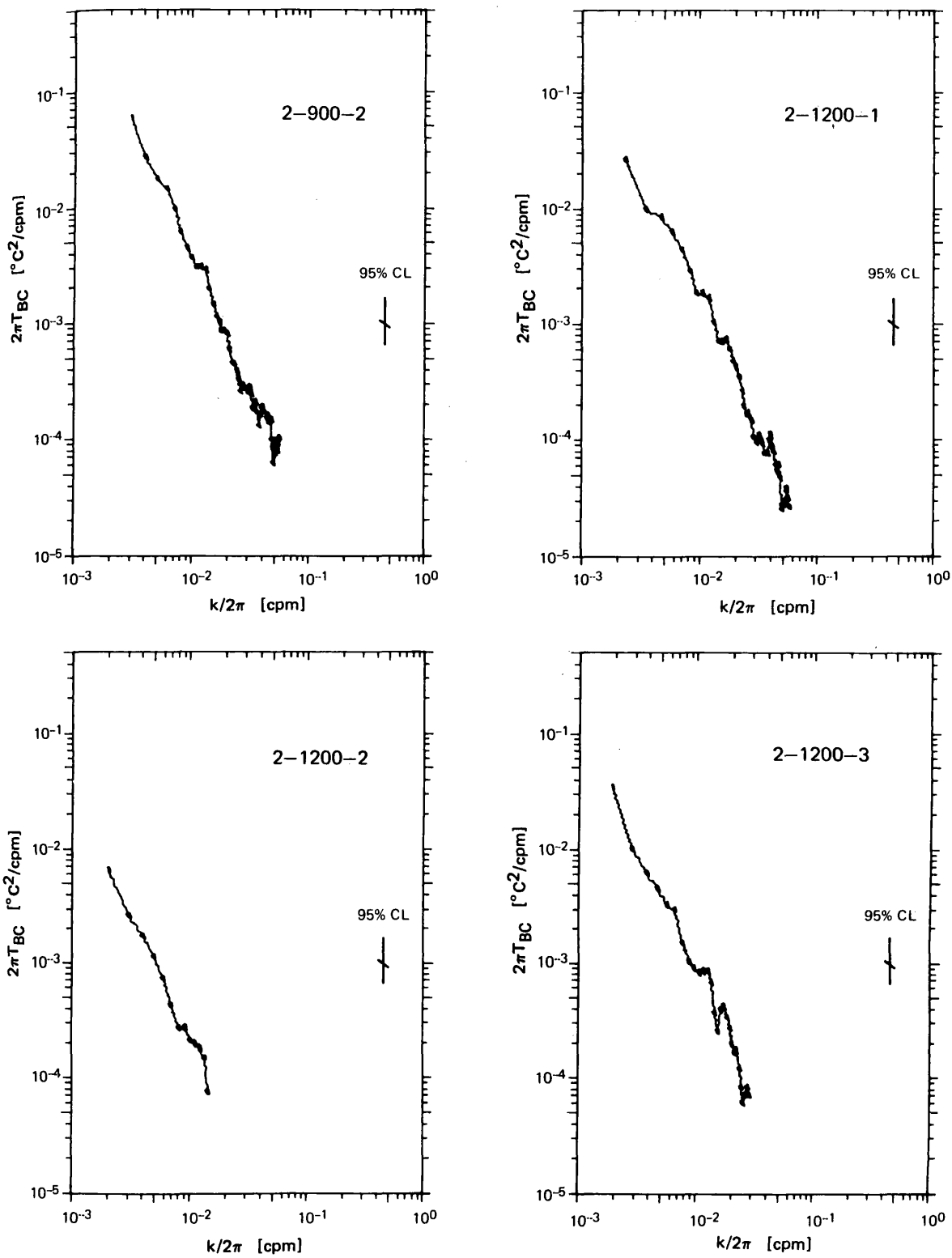


Fig. B1—Temperature power spectral density plots with 95% confidence limits (Continued)

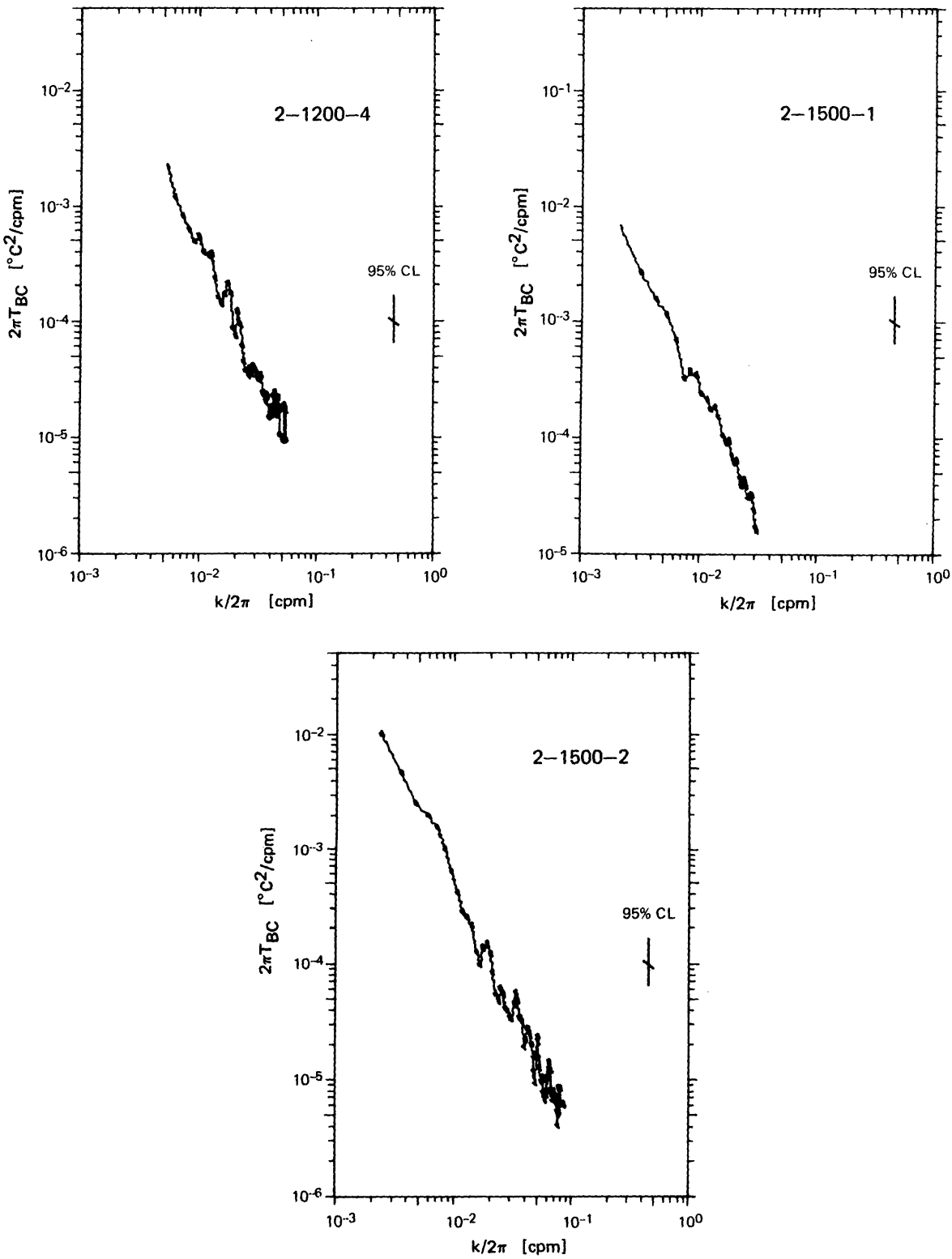


Fig. B1—Temperature power spectral density plots with 95% confidence limits (Continued)

## Appendix C
## INSTABILITY OF MEDIUM

On a small scale, the ocean is basically an unstable medium. The two dynamic mechanisms, internal waves and turbulence, in the presence of "layers" and "sheets," are probably the basic causes of this vertical and horizontal instability at depths greater than 100 m.

In the thermocline, the temperature decreases in a stepwise fashion with increasing depth. There appear to be isothermal "layers" on the order of 3-10 m separated by "sheets" of high gradient on the order of a meter or less wherein the temperature changes by about 0.1°C. The entire structure seems to deform in the presence of internal waves, so that if a temperature probe is maintained at a constant depth it will measure a series of nearly discrete temperature changes. In the case of a towed temperature sensor where the depth stability is related to the sea surface conditions, many extraneous temperature "jumps" occur. This is the medium instability referred to in the body of the report. The "sheet-layer" structure and temporal variability are shown in Fig. C1, which contains profile "snapshots" of the same water column showing the structural change during a 3-min period.

The steplike structure in the neighborhood of the towed temperature sensor changes considerably during the 13.7-min data segment. The extraneous temperature "jumps" encountered by the probe cause the squared coherency estimate of the temperature-depth correlation to be contaminated near 0.1 cpm. However, the estimates of the squared coherency at smaller wavenumbers are accurate, since it is the relatively stable mean temperature gradient which causes the temperature-vs-depth correlation in this range.

If one were to look at a shorter time series, the lower wavenumbers would be eliminated, but the squared coherency would better reflect the temperature-vs-depth correlation since the spatial interval over which the statistic is computed is more homogeneous. An example of this type of analysis is shown in Fig. C2, where the basic time series is 25.6 s. In this analysis, statistical significance is obtained by first averaging each consecutive pair of spectra to form a mini spectrum, removing the squared coherency, and then averaging 100 of these minispectra to obtain the grand spectrum.

In Fig. C3, the following information is apparent: (a) the raw temperature power density spectrum is seriously affected between $k$ = 0.06 cpm and $k$ = 0.2 cpm (presumably by vertical probe motion due to surface coupling); (b) the temperature and depth spectra are highly correlated in the same wavenumber range; (c) removing the squared coherency from the temperature spectrum reduces the overall energy in the affected wavenumber range, but not to a sufficient degree; and (d) the contamination in the temperature spectrum is virtually eliminated by means of the short (25.6-s) transform interval (at the expense of losing information at low wavenumbers.)

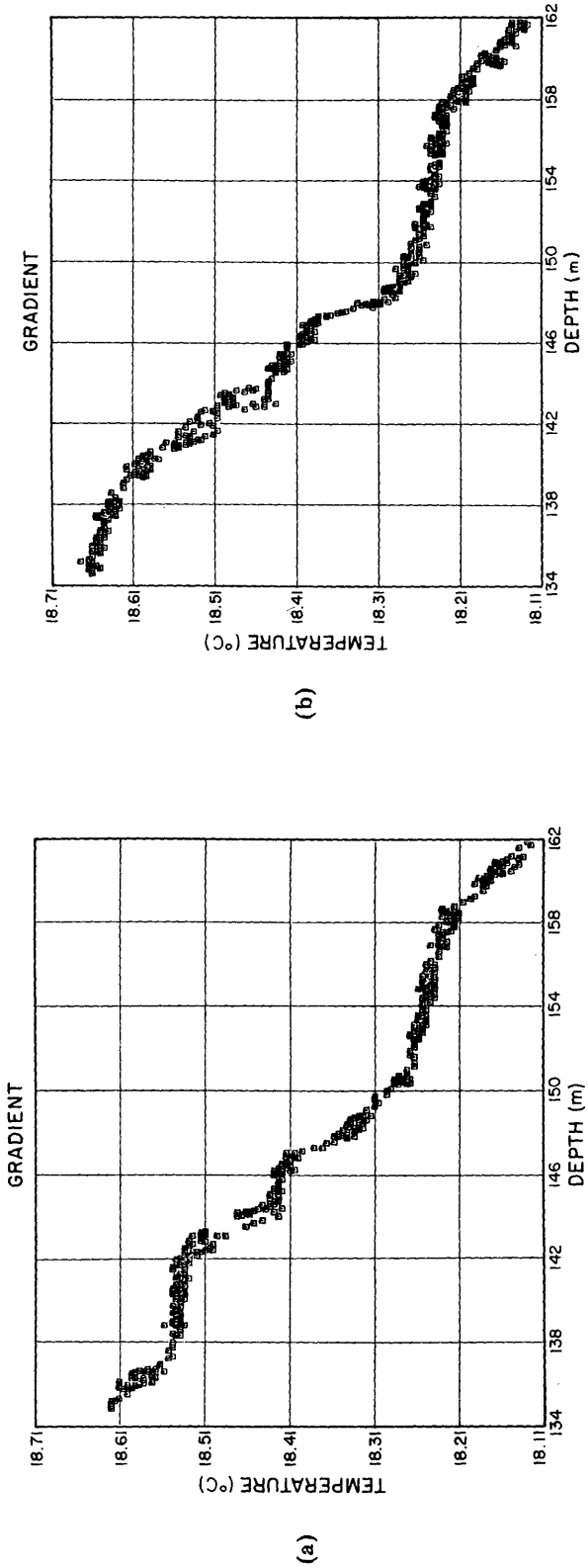


Fig. C1—Temperature structure change in 3 min

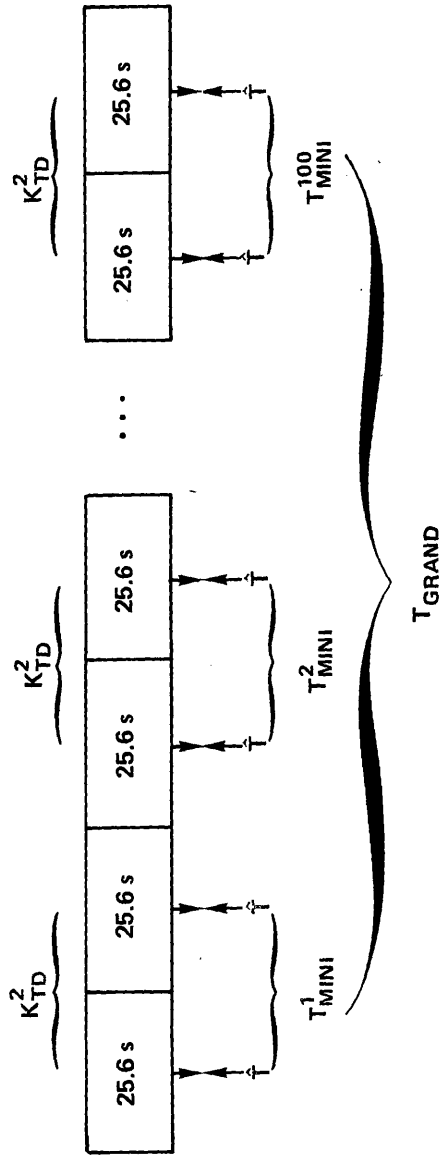


Fig. C2—Short-time series analysis to better remove temperature-vs-depth correlation.

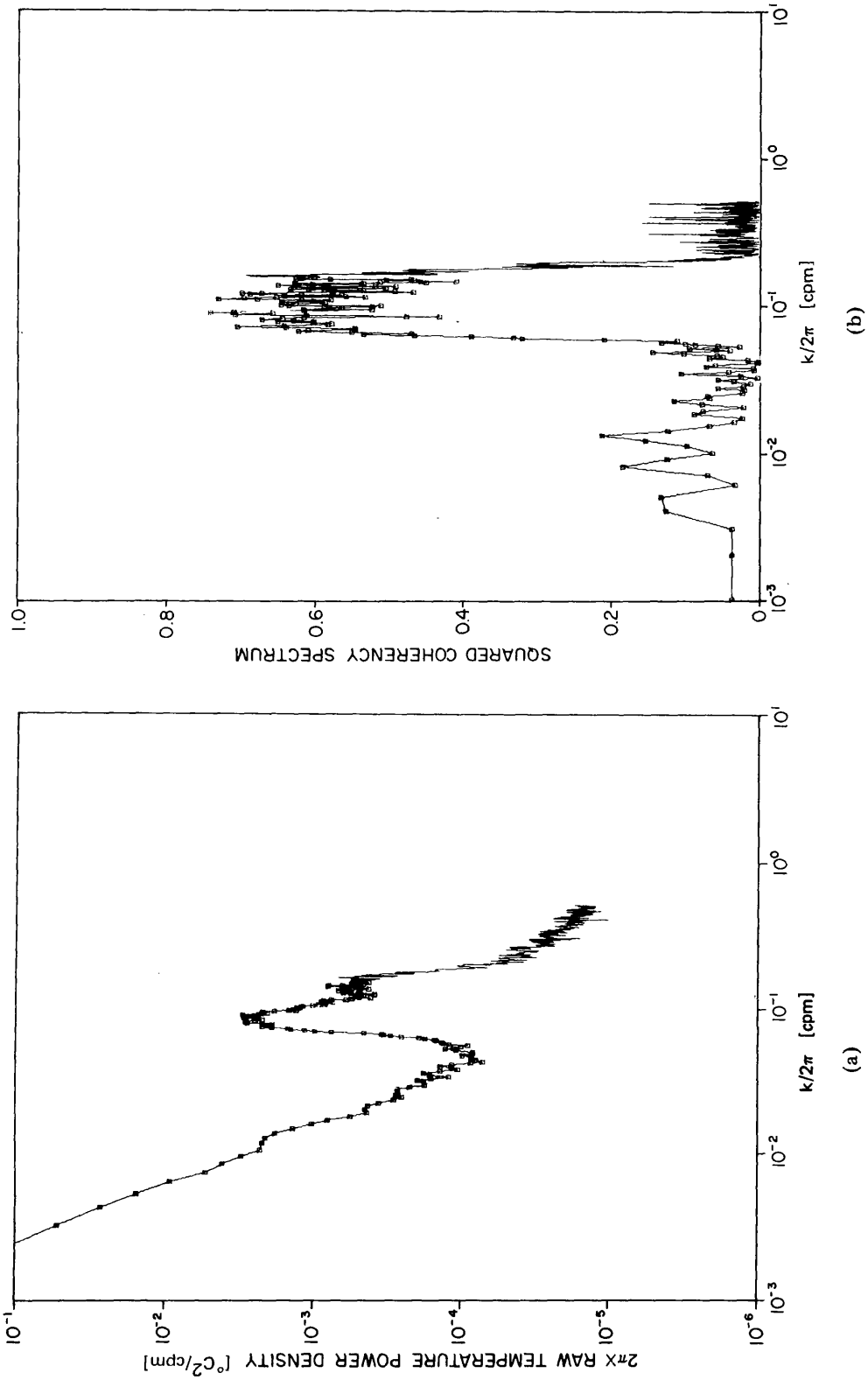
2πx RAW TEMPERATURE POWER DENSITY [°C²/cpm]
10⁻¹
10⁻²
10⁻³
10⁻⁴
10⁻⁵
10⁻⁶
10⁻³
10⁻²
10⁻¹
10⁰
10¹
k/2π [cpm]
(a)
SQUARED COHERENCY SPECTRUM
1.0
0.8
0.6
0.4
0.2
0
10⁻³
10⁻²
10⁻¹
10⁰
10¹
k/2π [cpm]
(b)

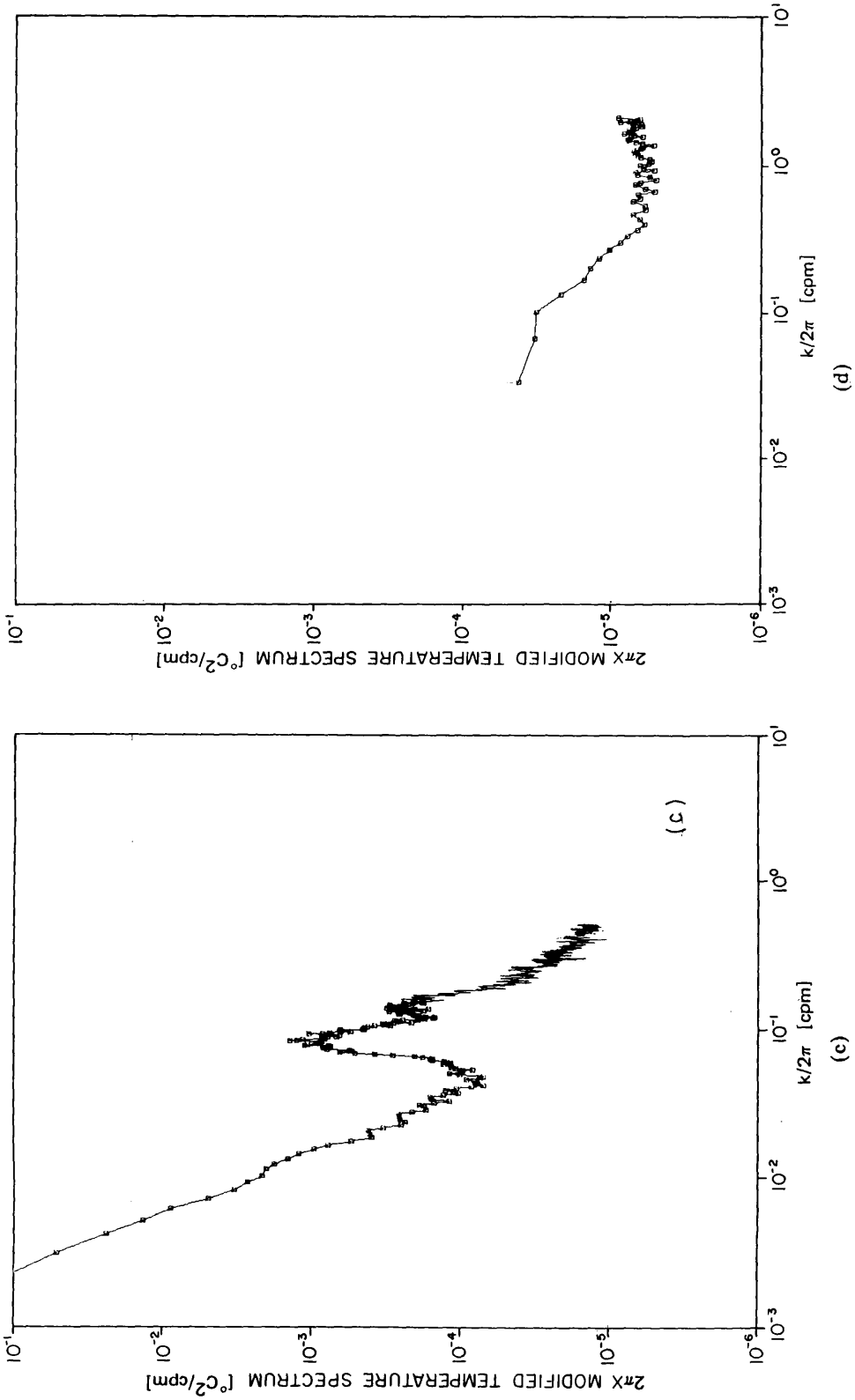


Fig. C3—(a) Raw temperature spectrum, (b) squared coherency spectrum, (c) modified temperature spectrum, and (d) spectrum resulting from short-time-series analysis

## SYMBOLS

| | |
|---|---|
| $V_I$ | Velocity spectrum in the inertial range |
| $V_{BI}$ | Velocity spectrum throughout the buoyancy-inertial range |
| $T_C$ | Temperature spectrum in the convective range |
| $T_{BC}$ | Temperature spectrum throughout the buoyancy-convective range |
| $k$ | Wavenumber |
| $k_b$ | High wavenumber cutoff for buoyancy effects |
| $N$ | Brunt-Väisälä frequency |
| $\epsilon$ | Net rate of spectral energy transfer |
| $\epsilon_0$ | Total rate of energy dissipation |
| $D_\theta$ | Total rate of dissipation of temperature variance |
| $B$, $C$, $\beta$ | Constants |
| $A_1$ | Coefficient of -5/3 term in equation for $T_{BC}(k)$ |
| $A_2$ | Coefficient of -3 term in equation for $T_{BC}(k)$ |